Phytochemistry 215 (2023) 113855

Contents lists available at ScienceDirect

Phytochemistry

journal homepage: www.elsevier.com/locate/phytochem

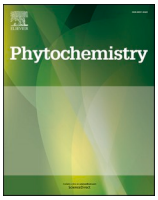

Synthetic and analytical routes to the L-amino acid conjugates of *cis*-OPDA and their identification and quantification in plants

Václav Mik [a,1], Tomáš Pospíšil [b,1], Federica Brunoni [c], Jiří Grúz [a], Vladimíra Nožková [b], Claus Wasternack [c], Otto Miersch [c], Miroslav Strnad [c], Kristýna Floková [c], Ondřej Novák [c], Jitka Široká [c,*]

[a] Department of Experimental Biology, Faculty of Science, Palacký University in Olomouc, Šlechtitelů 27, Olomouc, 783 71, Czech Republic
[b] Department of Chemical Biology, Faculty of Science, Palacký University in Olomouc, Šlechtitelů 27, Olomouc, 783 71, Czech Republic
[c] Laboratory of Growth Regulators, Palacký University in Olomouc & Institute of Experimental Botany AS CR, Šlechtitelů 27, Olomouc, 783 71, Czech Republic

ARTICLE INFO

Keywords:
Arabidopsis thaliana (Brassicaceae)
Wounding
Identification
Jasmonates
Cis-OPDA
Amino acid conjugates
Labeled compounds
Liquid chromatography
Tandem mass spectrometry

ABSTRACT

Cis-(+)-12-oxophytodienoic acid (*cis*-(+)-OPDA) is a bioactive jasmonate, a precursor of jasmonic acid, which also displays signaling activity on its own. Modulation of *cis*-(+)-OPDA actions may be carried out via biotransformation leading to metabolites of various functions. This work introduces a methodology for the synthesis of racemic *cis*-OPDA conjugates with amino acids (OPDA-aa) and their deuterium-labeled analogs, which enables the unambiguous identification and accurate quantification of these compounds in plants. We have developed a highly sensitive liquid chromatography-tandem mass spectrometry-based method for the reliable determination of seven OPDA-aa (OPDA-Alanine, OPDA-Aspartate, OPDA-Glutamate, OPDA-Glycine, OPDA-Isoleucine, OPDA-Phenylalanine, and OPDA-Valine) from minute amount of plant material. The extraction from 10 mg of fresh plant tissue by 10% aqueous methanol followed by single-step sample clean-up on hydrophilic–lipophilic balanced columns prior to final analysis was optimized. The method was validated in terms of accuracy and precision, and the method parameters such as process efficiency, recovery and matrix effects were evaluated. In mechanically wounded 30-day-old *Arabidopsis thaliana* leaves, five endogenous (+)-OPDA-aa were identified and their endogenous levels were estimated. The time-course accumulation revealed a peak 60 min after the wounding, roughly corresponding to the accumulation of *cis*-(+)-OPDA. Our synthetic and analytical methodologies will support studies on *cis*-(+)-OPDA conjugation with amino acids and research into the biological significance of these metabolites in plants.

1. Introduction

Jasmonates (JAs) are phytohormones contributing to growth and development control and are key regulators of defense reactions in response to biotic and abiotic stresses in plants (Wasternack and Hause, 2013). Chemically, JAs are jasmonic acid (JA)-like oxylipins containing cyclopentanone or cyclopentenone ring in their structure, which are synthesized from polyunsaturated fatty acids of plastid membranes (Wasternack and Feussner, 2018). JAs actions are mostly connected with gene expression induced by the interaction of a bioactive jasmonate with the COI1-JAZ (coronatine insensitive 1- jasmonate ZIM domain) co-receptor complex (Chini et al., 2007, 2016; Howe et al., 2018; Sheard et al., 2010). The jasmonate signaling is triggered by (+)-7-*iso*-jasmonoyl-L-isoleucine (JA-Ile) in vascular plants (Fonseca et al., 2009). However, in non-vascular plants, *Physcomitrium patens* and *Marchantia polymorpha* unable to synthesize JA-Ile (Stumpe et al., 2010; Yamamoto et al., 2015), other bioactive JAs were identified to be ligands of the COI1-JAZ co-receptor, namely isomers of dinor-12-oxo-phytodienoic acid (dn-*iso*-OPDA and dn-*cis*-OPDA) (Monte et al., 2018) and Δ^4-dn-OPDA (Kneeshaw et al., 2022) in *Marchantia*. The *cis*-(+)-12-oxophytodienoic acid (*cis*-(+)-OPDA) is a bioactive jasmonate present in all plant species, including non-vascular plants (Chini

* Corresponding author. Laboratory of Growth Regulators, Šlechtitelů 27, Olomouc, 783 71, Czech Republic.
E-mail addresses: vaclav.mik@upol.cz (V. Mik), tomas.pospisil@upol.cz (T. Pospíšil), federica.brunoni@upol.cz (F. Brunoni), jiri.gruz@upol.cz (J. Grúz), vladimira.nozkova@upol.cz (V. Nožková), cwastern@ipb-halle.de (C. Wasternack), omiersch@gmx.de (O. Miersch), miroslav.strnad@upol.cz (M. Strnad), kristyna.flokova@yahoo.fr (K. Floková), ondrej.novak@upol.cz (O. Novák), jitka.siroka@upol.cz (J. Široká).
[1] These authors contributed equally.

https://doi.org/10.1016/j.phytochem.2023.113855
Received 11 June 2023; Received in revised form 6 September 2023; Accepted 7 September 2023
Available online 9 September 2023

et al., 2023), predominantly recognized as a precursor of JA-Ile. *Cis*-(+)-OPDA synthesis (octadecanoid pathway, Fig. 1) is initiated by peroxidation of α-linolenic acid (18:3) (α-LA) from plastid membrane catalyzed by 13-lipoxygenase (13-LOX) to form (13*S*)-hydroperoxyoctadecatrienoic acid (13-HPOT). 13-HPOT is converted further by allene oxide synthase (AOS) to (13*S*)-12,13-epoxyoctadecatrienoic acid (12,13-EOT) from which *cis*-(+)-OPDA is cyclized by allene oxide cyclase (AOC). *Cis*-(+)-OPDA itself does not bind to the COI1-JAZ co-receptor complex (Thines et al., 2007). However, it can trigger gene expression independently from COI1 and perform various biological functions as reviewed in (Aleman et al., 2022; Liu and Park, 2021; Maynard et al., 2018). Some of these functions were linked to reactive electrophilic properties of α,β-unsaturated carbonyl moiety of *cis*-(+)-OPDA, e.g., role in defence responses (Park et al., 2013),

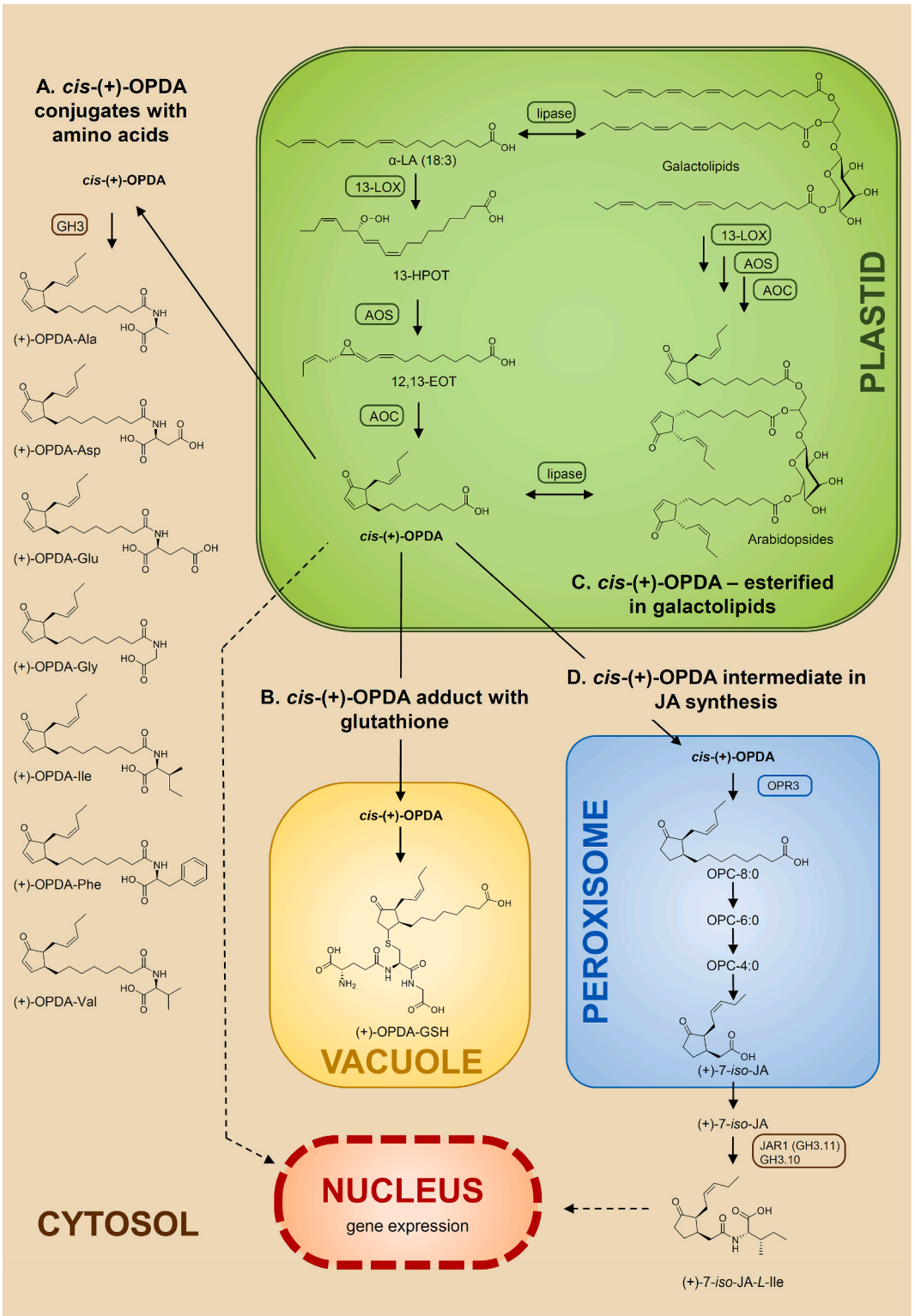

Fig. 1. *Cis*-(+)-OPDA synthesis and biotransformation pathways with their putative subcellular location. The scheme is based on (Bittner et al., 2022; Wasternack and Song, 2017).

themotolerance (Monte et al., 2020) or stomatal opening (Chang et al., 2023).

Plant hormones are highly active molecules, and their homeostasis in plants is tightly regulated. Modification of chemical structures alters their biological activity and determines their degradation, storage, or activation (Westfall et al., 2013). The amino acid conjugation of acidic phytohormones mediated by the GRETCHEN HAGEN 3 (GH3) acyl acid-amido synthetases is a conserved mechanism involved in the dynamic regulation of the cellular levels of JAs, auxins, and benzoates (Brunoni et al., 2020, 2023; Staswick et al., 2002, 2005; Westfall et al., 2016). Amino acid conjugation of auxins attenuates their bioactivity. In contrast, the conjugation of Glu to isochorismate leads to the formation of the precursor of salicylic acid and conjugation of Ile to JA is essential for the formation of the bioactive hormone (Jez, 2022). Thus, amino acid conjugation of phytohormones is a widespread metabolic regulation controlling plant hormone activity. Among JAs, the biotransformation of *cis*-(+)-OPDA and its biological consequences are far less explored compared to JA. *Cis*-(+)-OPDA conjugates with amino acids ((+)-OPDA-aa) (Fig. 1, A) were described in the literature recently. As an analog to JA-Ile, the *cis*-(+)-12-oxophytodienoyl-L-isoleucine ((+)-OPDA-Ile) was identified in wounded leaves of flowering *Arabidopsis thaliana* (*At*) (Floková et al., 2016) and some biological activity was attributed to this molecule (Arnold et al., 2016). Several *cis*-(+)-OPDA conjugates were putatively identified in *cis*-(+)-OPDA--treated rice cells. An increase in (+)-OPDA-Asp levels upon chitooligosaccharide application activating the pattern-triggered immunity and simulating biotic stress conditions was determined in rice cell culture (Shinya et al., 2022). *Cis*-(+)-OPDA form adducts with glutathione (γ-glutamyl-cysteinyl-glycine; GSH; Fig. 1, B), the most abundant thiol molecule in cells (Hasanuzzaman et al., 2017). The cyclopentenone ring of *cis*-(+)-OPDA undergoes Michael addition with the free thiol group of GSH (Davoine et al., 2006), and the resulting (+)-OPDA-GSH (also can be named as OPC-8:0-GSH) adducts are stored in vacuoles (Ohkama-Ohtsu et al., 2011). The reactivity of *cis*-(+)-OPDA with thiol groups is linked to cellular redox homeostasis maintenance (Knieper et al., 2022; Park et al., 2013) and the possible detoxification mechanism of accumulated *cis*-(+)-OPDA after stress (Ohkama-Ohtsu et al., 2011). *Cis*-(+)-OPDA has also been found esterified in galactolipids – Arabidopsides (Fig. 1, C), firstly identified in *At* (Stelmach et al., 2001) and later discovered in other plant species (Genva et al., 2019). Their role is hypothesized to be a storage form of rapidly available intermediates in the JA biosynthesis pathway (Genva et al., 2019; Stelmach et al., 2001). The principal pathway concerning *cis*-(+)-OPDA is leading to JA-Ile (Fig. 1, D), the chief jasmonate in vascular plants. The main JA biosynthesis pathway initiates in peroxisomes by reduction of *cis*-(+)-OPDA to (*Z*)-8-[3-oxo-2-(pent-2-enyl)cyclopentyl]octanoic acid (OPC-8:0) by OPDA reductase 3 (OPR3) followed by three cycles of β-oxidation shortening the carboxylic side chain ((*Z*)-6-[3-oxo-2-(pent-2-enyl)cyclopentyl]hexanoic acid, OPC-6:0; (*Z*)-4-[3-oxo-2-(pent-2-enyl)cyclopentyl]butanoic acid, OPC-4:0) and resulting in jasmonic acid, (+)-7-*iso*-JA. Conjugation to L-isoleucine in the cytosol catalyzed by JASMONATE RESISTANT1 (JAR1, GH3.11) and GH3.10 results in (+)-7-*iso*-JA-Ile (Delfin et al., 2022; Staswick and Tiryaki, 2004). However, another possible pathway converting *cis*-(+)-OPDA in three rounds of β-oxidation in peroxisome to 4,5-didehydro-JA and reduced by OPDA reductase 2 to (+)-7-*iso*-JA in the cytosol was revealed (Chini et al., 2018) (not illustrated in Fig. 1). The discovery of the OPR3 independent pathway challenged the previous JAs research performed on the opr3 single mutants as they can still synthesize JA-Ile, and therefore the biological activity of *cis*-(+)-OPDA cannot be distinguished from that of JA-Ile using these mutants.

The plant hormone quantitative analysis is usually based on sensitive and selective tandem mass spectrometry (MS/MS) (Cai et al., 2019; Novák et al., 2017; Šimura et al., 2018). As plant hormones are typically present in trace amounts in a complex matrix containing highly abundant substances (pigments, plant lipids, etc.), there is a considerable potential for matrix effects (primarily ion suppression) in the ion source of mass spectrometer (MS), and the analytes may not be detected despite using sensitive instrumentation (Furey et al., 2013). Coupling with liquid chromatography (LC) can provide separation of the analytes from matrix components and increase the sensitivity of MS detection. Furthermore, in sample preparation, besides an effective extraction aiming to obtain the highest amount of analyte and the lowest amount of matrix, a purification step using solid phase extraction (SPE) may be included to reduce the amount of matrix in the sample before the LC-MS/MS analysis (Tarkowská et al., 2014). To compensate for analyte losses during sample preparation and reduce the effect of the matrix, the isotopically labeled internal standards (IS) are employed for accurate MS quantification (Furey et al., 2013). The qualitative analysis applies criteria for chromatography and MS, and the unambiguous identification of the structure at the highest confidence level can be only performed using an authentic analytical standard (Milman, 2015; Rochat, 2017).

This work aimed to optimize a synthetic route to obtain authentic OPDA-aa standards and their isotopically labeled analogs essential for development of an analytical method for OPDA-aa identification and accurate quantification in plants. At the same time, we have developed an LC-MS/MS method and a sample preparation step that allow for the sensitive determination of OPDA-aa. The results of our work will further provide tools for studying the conditional occurrence and biological roles of OPDA-aa in plants.

2. Results and discussion

2.1. *Cis*-OPDA synthesis

Synthesis of *cis*-12-oxophytodienoic acid (*cis*-OPDA) (**3**) and its deuterium labeled analog (17,17,18,18,18-d_5)-*cis*-OPDA (**4**) was achieved by enzymatic conversion of α-LA (**1**) and (17,17,18,18,18-d_5)-α-LA (**2**) (Fig. 2). Enzymatic transformation of α-LA acid into *cis*-OPDA, which naturally occurs in the plant plastids (Fig. 1), requires the sequential action of three enzymes – 13-LOX, AOS, and AOC. Firstly, 13-LOX catalyzes dioxygenation of **1** at the C13 position into 13-HPOT, which AOS further transforms into 12,13-EOT. This highly unstable allene oxide can be subjected to the stereo-specific cyclization catalyzed by AOC, leading to the formation of *cis*-(+)-OPDA, or can undergo spontaneous non-enzymatic cyclization leading to the formation of (+/−)-*cis*-OPDA mixture (racemic mixture) or hydrolysis into α- and γ-ketol. In this regard, the last enzymatic step is essential, as it determines the reaction's overall yield and the desired product's chiral purity. The enzymatic apparatus required for converting α-LA into *cis*-OPDA can be isolated from lipid-free flax seed powder (Zimmerman and Feng, 1978). The reaction provides *cis*-OPDA in reasonable yields. However, only racemic *cis*-OPDA is obtained due to the insufficient activity of AOC (Kajiwara et al., 2012). A much higher reaction yield and dramatic increase of stereo-selectivity, forming natural *cis*-(+)-OPDA enantiomer, can be achieved by the addition of recombinant AOC to the flax seed extract (Kajiwara et al., 2012) or by optimized enzymatic cascade based on recombinant proteins (Löwe et al., 2020).

Conversion of sodium salts **1** and **2** into **3** and **4**, respectively (Fig. 2), was achieved by lipid-free flax seed powder extract according to a slightly modified protocol (Zimmerman and Feng, 1978). The isolation yield of **3** and **4** was around 20%, and the compounds were obtained with a high diastereomeric ratio (>99:1 - *cis*:*trans*, according to the NMR in Supplementary data). Measurement of specific optical rotation of **3** ($[\alpha]_D^{20} = +8$) showed a slightly enriched mixture of enantiomers have been prepared since the obtained value is far away from reported values of pure *cis*-(+)-OPDA ($[\alpha]_D^{20} = +104$ (Grieco and Abood, 1989), $[\alpha]_D^{28} = +127$ (Ainai et al., 2003), $[\alpha]_D^{25} = +140$ (Kajiwara et al., 2012)).

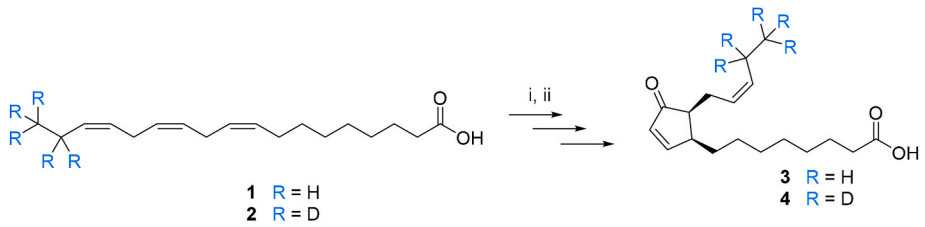

Fig. 2. Enzymatic synthesis of *cis*-OPDA and (17,17,18,18,18)-d_5-*cis*-OPDA. Reagent and conditions: i) 1 mol/l NaOH, room temperature, 15 min, then Sörensen's phosphate buffer (pH = 7), room temperature, 20 min; ii) extract from lipid-free flax seed powder, Sörensen's phosphate buffer (pH = 7), room temperature, 2 h.

2.2. Synthesis of cis-OPDA conjugates with amino acids

In comparison to the previously published synthesis of *cis*-OPDA-Ile (Floková et al., 2016), conjugation of **3** or **4** with amino acids took place this time in strictly anhydrous conditions (Fig. 3). Carboxylic group of **3** and **4** was also as in previous case activated by formation of mixed anhydride by the reaction with isobutyl chloroformate (IBCF) and TEA (trimethylamine) in dry THF (tetrahydrofuran) at −10 °C. Removal of salts by filtration provided clear solutions of **5** and **6,** which were dropwise added to the solutions of silylated amino acids **8a-g** at 0 °C. These were obtained by the reaction of **7a-g** (Gly, Ala, Val, Ile, Phe, Asp, Glu) with TMS-Cl (trimethylsilyl chloride) and TEA in acetonitrile under reflux and filtration of resulting salts upon gradual cooling to room temperature. Conjugation occurred at 0 °C for 2 h, followed by acidification of reaction mixtures with 1 mol/l HCl and extraction with chloroform, which provided desired compounds **9a-g** and their labeled analog **10a-g** with yields ranging from 23 to 82%. Although the conjugation of racemic *cis*-OPDA to chiral amino acids should result in the formation of potentially separable diastereomers, we could not separate them. *Cis*-OPDA (**3**) is extremely sensitive to acids and bases, which may lead to the epimerization at C13 forming undesirable *trans* isomer or even rearrangement of the double bond leading to the more thermodynamically stable cyclopentenone (Grieco and Abood, 1989). Using anhydrous and mild conditions in the conjugation step, only negligible changes in the *cis*:*trans* OPDA epimers ratio were observed (>95:5, *cis*:*trans* according to NMR in Supplementary data).

2.3. LC-MS/MS method development

The OPDA-aa form ions in positive and negative electrospray ionization (ESI) mode. The positive ionization mode provided higher intensities and signal-to-background noise ratios of analyte peaks compared to the negative ionization in full scan mode. The fragmentation of protonated molecular ions $[M + H]^+$ of OPDA-aa was performed at four fixed collision energies (CEs; 10, 20, 30, and 40 eV). The two most intensive fragments specific for each compound were selected as diagnostic ions to establish the multiple reaction monitoring transitions (MRM) and the CEs were optimized (Table 1). The fragmentation spectra at 20 eV of OPDA-aa and ISs are depicted in Supplemental Figs. S1–S7. For OPDA-aa, the characteristic fragment was *m/z* 275 (or *m/z* 280 for d_5-OPDA-aa of ISs), which is an ion of *cis*-OPDA (*m/z* 293) with neutral loss of H_2O (NL 18 Da) or a neutral loss of the amino acid. Other intensive fragments corresponded to the protonated ions of amino acids (*m/z* 89.9 – Ala, *m/z* 76.0 - Gly, *m/z* 133.9 – Asp, *m/z* 148 - Glu) or fragments of the amino acids with a loss of $H_2O + CO$ (NL 46 Da) (*m/z* 86 for Ile, *m/z* 120 for Phe, *m/z* 72 for Val). Highly abundant ions were also the OPDA-aa with loss of $H_2O + CO$ (NL 46 Da) or 2 $H_2O + CO$ for Asp (NL 64 Da); however, these ions were excluded due to low specificity to the structure. In comparison, an optimized method for the determination of OPDA-Ile employed MRM in negative ionization mode corresponding to the deprotonated molecular ion of OPDA-Ile and the deprotonated Ile (404 > 130) (Floková et al., 2016). Furthermore, using predicted molecular and fragment ions (*m/z* corresponding to deprotonated amino acids) 19 OPDA-aa conjugates were scanned in negative ionization mode (Shinya et al., 2022).

The separation of *cis*-OPDA and OPDA-aa (Fig. 4) was achieved following gradient and chromatographic conditions set for the separation of acidic plant hormones (abscisates, auxins, JAs, and salicylic acid) (Široká et al., 2022), which enabled the determination of all simultaneously in one LC run (Supplemental Fig. S8).

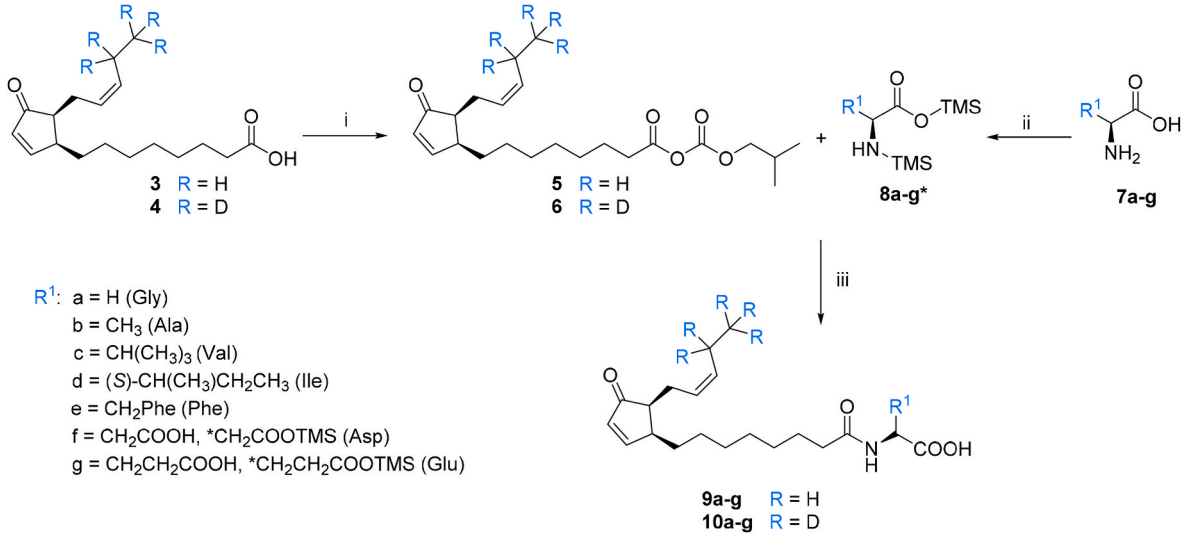

Fig. 3. Synthesis of amino acid conjugates of *cis*-OPDA and (17,17,18,18,18,18)-d_5-*cis*-OPDA. Reagent and conditions: i) IBCF, TEA, THF, −10 °C, 30 min; ii) TMS-Cl, TEA, acetonitrile, reflux; iii) 0 °C, 2 h, then 1 mol/l HCl, room temperature, 10 min * - side chain carboxylic groups of Asp and Glu were also protected by TMS.

Table 1
LC-MS/MS method parameters.

Analyte	Abbreviation	IS	Diagnostic MRM[a] (CE; eV)	MRM IS[a] (CE; eV)	Ionization	Rt; min[b]	Linear range (pmol)	LOD (fmol)[c]	pK_a[d]
cis-12-oxophytodienoyl-L-alanine	OPDA-Ala	d_5-OPDA-Ala	364.3 > 275.1 (22)[e] 364.3 > 90.0 (20)	369.3 > 280.0 (22) 369.3 > 89.9 (20)	$[M+H]^+$	13.32 ± 0.01	0.005–5	1	4.1
cis-12-oxophytodienoyl-L-aspartate	OPDA-Asp	d_5-OPDA-Asp	408.3 > 275.3 (22)[e] 408.3 > 134.1 (22)	413.2 > 280.0 (22)	$[M+H]^+$	13.33 ± 0.01	0.005–5	2	3.7
cis-12-oxophytodienoyl-L-glutamate	OPDA-Glu	d_5-OPDA-Glu	422.3 > 275.3 (22)[e] 422.3 > 148.1 (22)	427.2 > 280.0 (26)	$[M+H]^+$	13.04 ± 0.01	0.005–5	2	3.6
cis-12-oxophytodienoyl-L-glycin	OPDA-Gly	d_5-OPDA-Gly	350.2 > 275.0 (22)[e] 350.2 > 76.0 (24)	355.2 > 280.0 (12)	$[M+H]^+$	13.11 ± 0.01	0.005–5	2	4.1
cis-12-oxophytodienoyl-L-isoleucine	OPDA-Ile	d_5-OPDA-Ile	406.2 > 86.1 (36)[e] 406.2 > 275.1 (28)	411.2 > 86.1 (30)	$[M+H]^+$	14.35 ± 0.01	0.005–5	1	4.3
cis-12-oxophytodienoyl-L-phenylalanine	OPDA-Phe	d_5-OPDA-Phe	440.3 > 120.1 (40)[e] 440.3 > 275.2 (30)	445.3 > 120.1 (32)	$[M+H]^+$	14.62 ± 0.01	0.005–5	2	4.1
cis-12-oxophytodienoyl-L-valine	OPDA-Val	d_5-OPDA-Val	392.3 > 72.2 (40)[e] 392.3 > 275.1 (24)	397.3 > 280.0 (20)	$[M+H]^+$	14.01 ± 0.01	0.005–5	1	4.2

[a] Optimized on standards.
[b] Means ± standard deviation (s.d.), (n = 10).
[c] Limit of detection: S/N > 3, expressed as an amount of substance injected.
[d] Predicted in chemicalize.com.
[e] Reference diagnostic ion.

2.4. Optimization of sample preparation method

The OPDA-aa are weak acids (pK_a between 3.6 and 4.3, Table 1) that can be retained both on reverse phase and ion exchange sorbents. The generic ion exchange SPE protocols operate on the edges of the pH range (e.g., 2% formic acid or 5% ammonium hydroxide), and the analytes containing amide (e.g., conjugates with amino acids) or ester (e.g., conjugates with glucose) bonds in the structure may chemically degrade under these conditions (Šimura et al., 2018). To evaluate the stability during sample preparation, the standard solution of analytes was incubated for 30 min in 2% formic acid in methanol, 5% ammonium hydroxide in methanol, and methanol as control. The stability of all seven OPDA-aa in 2% formic acid and 5% ammonium hydroxide was above 85% (Supplemental Fig. S9).

The retention of analytes on ion exchange MAX (mixed-mode anion exchange) and reverse phase HLB (hydrophilic-lipophilic balanced) SPE sorbents was tested on standards applying generic Waters protocols. The mean purification recovery of OPDA-aa on a MAX and HLB column was 29% and 92%, respectively (Supplemental Fig. S10).

The effect of the organic solvent (methanol) content in the extraction solution on the process efficiency (PE) was evaluated using 10 mg *Arabidopsis thaliana* leaf matrix and HLB columns. The average PEs of the OPDA-aa in plant extracts in 10–25–50% aqueous (aq.) methanol were as follows 82%, 63%, and 62% (Supplemental Fig. S11). The protocol was therefore continued with 10% methanol as the extraction solvent. In comparison, Floková et al. (2016) used 25% aq. methanol to extract OPDA-Ile and achieved a PE of about 50% using 50 mg of plant tissue (24-day-old *At*) due to a higher amount of co-extracted compounds, decreasing the capacity of SPE sorbent.

Including an acidification step to increase retention of the acidic plant hormones in course of the sample purification on HLB sorbent was also employed by Floková et al. (2014), Novák et al. (2012) and Turečková et al. (2009). The effect of the implementation of an acidification step during sample preparation on HLB sorbent to PE of OPDA-aa was tested using (1) extraction of matrix samples in 10% aq. methanol and no acidification during the SPE, (2) extraction of matrix samples in 10% aq. methanol including preconditioning with 0.1% formic acid in water (Floková et al., 2014), (3) extraction of matrix samples in 10% aq. methanol and acidification of the plant extract before loading to SPE (adjusted to pH 2.6 by 1 mol/l hydrochloric acid)

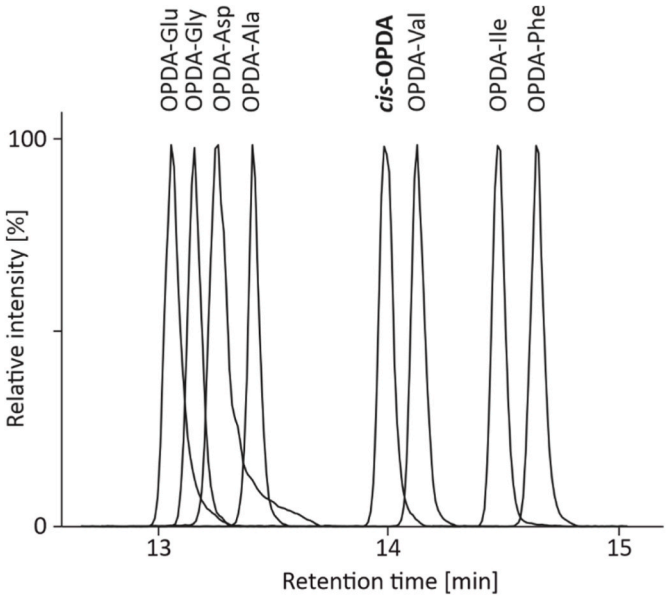

Fig. 4. LC-MS/MS separation of *cis*-OPDA and OPDA-aa conjugates.

Table 2
Validation parameters.

Analyte	Method Accuracy/Precision[a]			ME[a,b]	RE[a,b]	PE[a,b]
Spike	0.05 pmol	0.5 pmol	5 pmol			
OPDA-Ala	112.00/5.64	90.54/5.15	102.28/6.80	37.20 ± 4.11	86.93 ± 6.90	32.26 ± 2.61
OPDA-Asp	107.12/11.06	91.21/9.80	94.51/11.11	53.40 ± 3.43	91.07 ± 7.49	48.48 ± 4.16
OPDA-Glu	100.60/11.49	85.58/10.27	96.92/7.36	32.97 ± 2.05	96.83 ± 1.02	31.84 ± 0.36
OPDA-Gly	108.09/13.91	152.57/6.13	191.09/7.38	36.51 ± 5.89	85.54 ± 10.51	30.76 ± 4.18
OPDA-Ile	108.15/5.14	99.67/6.01	110.84/4.70	70.12 ± 8.23	95.98 ± 18.24	67.22 ± 13.14
OPDA-Phe	95.479/12.64	102.05/5.64	113.51/5.46	67.72 ± 8.40	92.05 ± 9.58	62.23 ± 6.62
OPDA-Val	95.19/9.28	104.09/7.17	105.50/6.71	49.40 ± 2.67	102.10 ± 10.26	50.45 ± 5.15

[a] Estimated by spiking of 10 mg 30-day-old *Arabidopsis thaliana* leaves samples in four replicates (n = 4).
[b] Means ± s.d.

similarly as (Novák et al., 2012) and (4) acidic extraction of matrix samples with 1 mol/l formic acid in 10% aq. methanol similarly as (Široká et al., 2022). All approaches provided similar average PE values of 60%, 59%, 54%, and 54% in experiments (1), (2), (3), and (4), respectively (Supplemental Fig. S12). The final conditions were set as approach (2) as this method was previously established for stress-induced acidic plant hormones, including JAs (Floková et al., 2014). Importantly, the experiment (2) also allows simultaneous sample preparation for OPDA-aa and JAs analysis in one step.

2.5. Method validation

The method for OPDA-aa determination was validated in terms of accuracy and precision. The method accuracies were within the 85–115% range, except for OPDA-Gly, and the method precisions were lower than 15% for all OPDA-aa (Table 2). The OPDA-Gly, despite the accuracy within the validation limits at the first concentration level, failed to be quantified accurately at the second and third concentration levels. This may be caused by a possible interfering compound at the retention time (Rt) of OPDA-Gly.

The mean PE of all OPDA-aa was 46% in the validation experiment. To overall PE negatively contributed the matrix effects (MEs), which were, on average, 50%. Unlike the ME, the losses during sample preparation, represented by recovery (RE), were relatively low, as the average RE was 92% (Table 2). The high MEs may be caused by the elution of the OPDA-aa at the end of the chromatographic gradient together with other non-polar compounds from the plant matrix (e.g., plant lipids).

2.6. Identification and quantification of (+)-OPDA-aa conjugates in wounded Arabidopsis thaliana leaves

The 30-day-old *At* plants were mechanically wounded by pinching with laboratory forceps and the whole injured leaves were collected at 0, 5, 15, 30, 60, and 180 min after wounding. The harvested samples were processed and profiled for endogenous JAs: *cis*-(+)-OPDA, (+)-OPDA-aa, JA, its precursors (OPC-8:0, OPC-6:0, OPC-4:0) and JA-Ile.

As there are no regulatory requirements in plant hormone qualitative analysis, for identification of the (+)-OPDA-aa in wounded *At*, the minimum criteria for chromatographic and MS confirmation issued by the World Anti-Doping Agency (WADA) were adopted (Technical document TD2023IDCR). For each (+)-OPDA-aa, the relative retention time (RRt) to its proper IS was calculated, and the tolerance limit was applied. Simultaneously, two diagnostic MRM transitions were acquired for each (+)-OPDA-aa (Table 1), their relative abundances (RAs) were calculated, and the tolerance intervals were applied. Except for (+)-OPDA-Ala, only one MRM was acquired for each IS. Supported by the RRts and RAs within the tolerance limits, the (+)-OPDA-Asp, (+)-OPDA-Glu, (+)-OPDA-Ile, (+)-OPDA-Phe, and (+)-OPDA-Val were identified and subsequently quantified in *At* wounded samples. The (+)-OPDA-Gly was not identified because the RAs were out of the tolerance range. This might be caused by an interfering compound of the same Rt providing a different rate of diagnostic and reference diagnostic MRM (Supplemental Fig. S13), which might have also been an issue during the validation. Nevertheless, RRts of (+)-OPDA-Gly peak agreed with the requirements for chromatography. Interestingly, the RAs of (+)-OPDA-Ala were also out of the tolerance limits, however, this was also the case with IS d_5-OPDA-Ala, where two diagnostic MRMs containing the same structural fragments were acquired (Supplemental Fig. S14). An equal concentration would be obtained if the levels were quantified using the MRMs of corresponding structural fragments of analyte and IS. The accumulation profile of (+)-OPDA-Ala in wounded *At* corresponds to the profiles of other identified (+)-OPDA-aa (Supplemental Fig. S15). The RRt fitted into the tolerance limits for (+)-OPDA-Ala.

The increase of JAs endogenous levels upon wounding has been recorded before (Stintzi et al., 2001; Weber et al., 1997). The time-course accumulation of (+)-OPDA-aa shows a maximum at 1 h after wounding, which roughly corresponds to the time-course of *cis*-(+)-OPDA in this experiment (Fig. 5). As in case of JA, its precursors (OPC-8:0, OPC-6:0, OPC-4:0) and JA-Ile accumulated 1 h after wounding (Supplemental Fig. S16). Interestingly, the profiles of JAs accumulation in response to mechanical wounding reported in literature differ between the studies published. Compared to our results, some studies on *At* Col-0 demonstrate maxima in wounded leaves at 30 min for JA (Floková et al., 2014), 60 min for JA and *cis*-(+)-OPDA (Koo et al., 2009) and/or 90 min for JA and 6 h for *cis*-(+)-OPDA after wounding (Reymond et al., 2000). The differences may stem from different experimental settings (e.g., the extent of leaf damage).

The levels of the (+)-OPDA-aa were in range 1–10 pmol/g of fresh weight (fr. wt) from the highest amount of (+)-OPDA-Glu > (+)-OPDA-Phe > (+)-OPDA-Ile > (+)-OPDA-Asp to lowest level of (+)-OPDA-Val (Fig. 5). A similar concentration range was reported for mechanically wounding-induced accumulation of (+)-OPDA-Ile in rosette leaves of *At* entering the final flowering stage on the main apex (29–39-day old), with the peak accumulation at 2 h post-wounding (Floková et al., 2016).

Besides the wounding-induced stress, OPDA-aa have also been investigated concerning the biotic stress responses. Out of 19 putatively identified OPDA-aa following OPDA exogenous treatment of rice cell culture, the (+)-OPDA-Asp was recently detected in rice cells after application of chitin oligosaccharide, a biotic stress response activator (Shinya et al., 2022).

Overall, our results suggest that *cis*-(+)-OPDA can be conjugated to various amino acids and this metabolic pathway is elicited by mechanical wounding. Hypothetically, the accumulated (+)-OPDA-aa may directly activate the COI1-JAZ co-receptor complex, or they can act in a COI1-independent manner similarly as reported for OPDA-Ile (Arnold et al., 2016) via e.g., their reactive electrophilic α,β-unsaturated carbonyl group (Knieper et al., 2022). Also, (+)-OPDA-aa can be temporary storage of *cis*-(+)-OPDA or indirectly activate the COI1-JAZ complex, due to hydrolysis to *cis*-(+)-OPDA and following JA-Ile synthesis. The signaling activity of *cis*-(+)-OPDA-aa and the role of *cis*-(+)-OPDA amino acid conjugation in plants will be the subject of future biological studies.

3. Concluding remarks

Here, we report a methodology for the synthesis of seven OPDA conjugates with amino acids as analytical standards and their labeled analogs used as IS, concurrently with the development and validation of

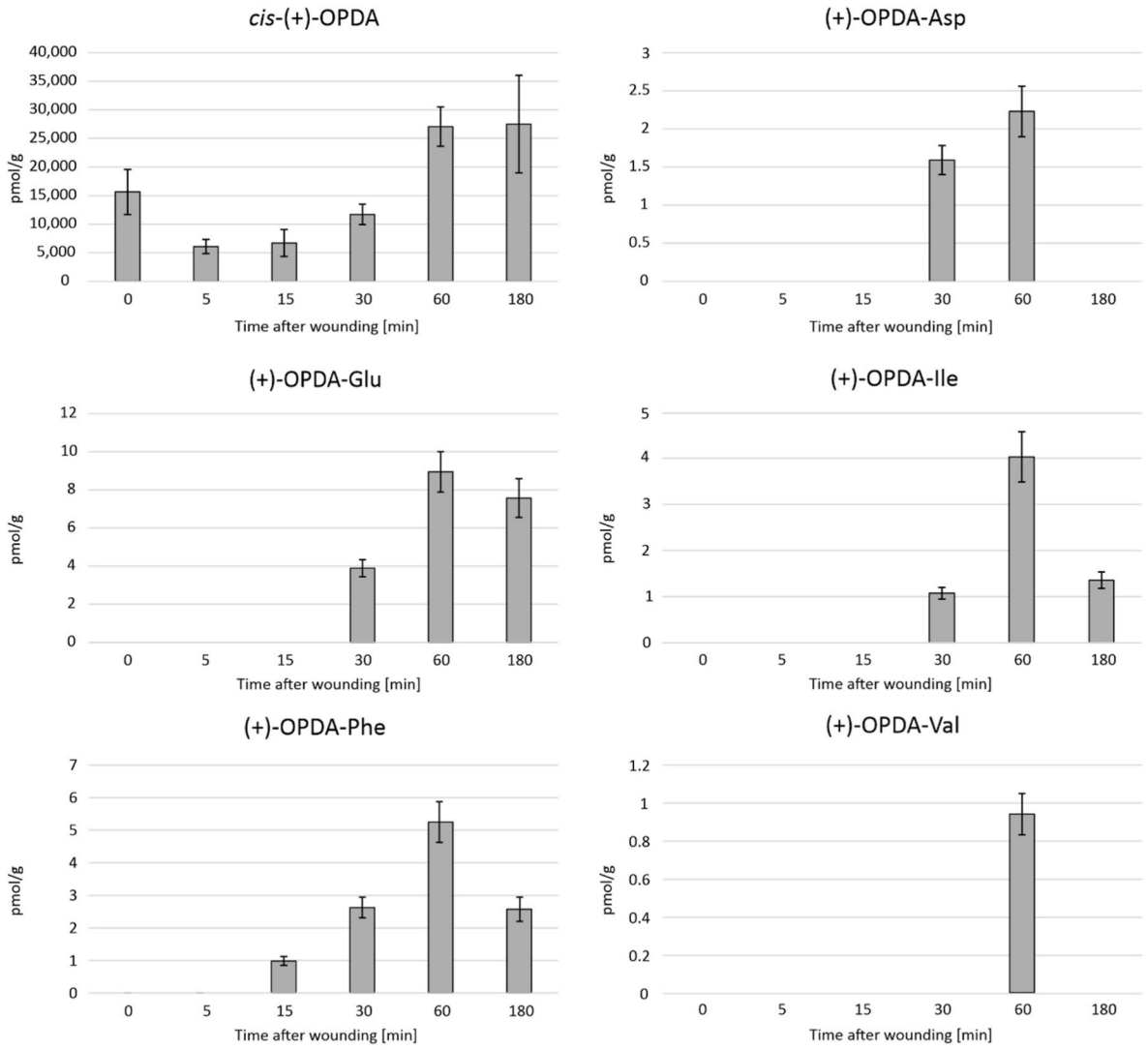

Fig. 5. Time–course accumulation of *cis*-(+)-OPDA and (+)-OPDA-aa. The results in 30-day-old *Arabidopsis thaliana* leaves mechanically wounded with forceps and collected 0, 5, 15, 30, 60, and 180 min after wounding. Time 0 min represents not wounded leaves from not-wounded plants. The bars are means ± s.d. (n = 6). The content of *cis*-(+)-OPDA and (+)-OPDA-aa is expressed in pmol/g fr. wt.

an analytical procedure comprising sample extraction and SPE-based purification prior to LC-MS/MS identification and accurate quantification in plants. Application of the method led to the identification of five (+)-OPDA-aa in wounded *At* leaves with a time-course reminiscent of *cis*-(+)-OPDA. Our results showed the accumulation of (+)-OPDA-aa under wounding stress and demonstrate the biotransformation of *cis*-(+)-OPDA to amino acid conjugates *in vivo* under physiological conditions.

4. Experimental

4.1. Synthesis - general experimental procedures

Common reagents and solvents were purchased from commercial sources (Sigma-Aldrich, St. Luis, MO, USA; VWR, LachNer) and used without further purifications. Deuterium labeled linolenic acid (17,17,18,18,18-d_5) was obtained from Cambridge Isotope Laboratories Inc. (Tewksbury, MA, USA). Flax seeds (*Linum usitatissimum* L.) of Raciol and Astella varieties were purchased from Agritec (Šumperk, Czech Republic). Thin-layer chromatography was performed on silica gel plates Silica F254, 200 μm (VWR). The spots were visualized by staining with basic potassium permanganate (1.5 g $KMnO_4$, 10 g K_2CO_3, 1.25 ml 10% NaOH, 200 ml water). The compounds were purified on a Prep-C18 LC column (100 × 21.2 mm, particle size 5 μm) using 1290 Infinity II LC/MSD preparative system with UV detector 1260 Infinity II and single quadrupole MS with electrospray ionization LC/MSD all from Agilent (Agilent Technologies, Santa Clara, CA, USA). The mobile phases consisted of 0.1% formic or acetic acid in water as an aq. phase and methanol or acetonitrile as an organic phase, the flow rate was set to 20 ml/min and the column was maintained at room temperature. Spectrometric purity and mass of the compounds were determined using the AQUITY UPLC® H-Glass system on Symmetry C18 column (150 × 2.1 mm, particle size 5 μm) linked simultaneously to ACQUITY UPLC PDA detector and single quadrupole MS QDa all from Waters (Waters, Milford, MA, USA). Specific optical rotation $[\alpha]_D^{20}$ was measured with a polarimeter PolAAR 2001 (Optical Activity Ltd., Ramsey, Huntingdon, UK) upon dissolving the sample in chloroform. ^{1}H and ^{13}C NMR spectra were recorded at 500/125 MHz on ECA-500 or at 400/100 MHz on ECZ/R-400 spectrometers (Jeol, Tokyo, Japan). Samples were dissolved in $CDCl_3$ and chemical shifts were calibrated to the residual solvent peak (δ = 7.26 ppm for ^{1}H and δ = 77.0 for ^{13}C). The accurate masses of standards were recorded upon direct injection of standard solutions using a hybrid quadrupole time of flight (QTOF) high resolution mass spectrometer (HRMS) SYNAPT G2-Si (Waters, Manchester, UK)

operating in positive ion mode.

4.2. Synthesis

4.2.1. Synthesis of 8-[(1S*,5S*)-4-oxo-5-((Z)-pent-2-en-1-yl)cyclopent-2-en-1-yl]octanoic acid (3, cis-OPDA) and 8-[(1S*,5S*)-4-oxo-5-((Z)-pent-2-en-1-yl-4,4,5,5,5-d_5)cyclopent-2-en-1-yl]octanoic acid (4, (17,17,18,18,18-d_5)-cis-OPDA)

The title compounds were prepared according to the literature procedure (Zimmerman and Feng, 1978). The spectral data are consistent with those reported in the literature.

3: pale yellow oil, yield 20%, UPLC-UV/VIS RT, purity (min., %): 24.79, 95.0; ESI$^+$-MS *m/z* (rel. int. %, ion): 293.3 (100, $[M+H]^+$). ^{1}H-NMR (400 MHz, $CDCl_3$) δ (ppm): 0.96 (t, $J = 7.5$ Hz, 3H), 1.12–1.16 (m, 1H), 1.31–1.41 (m, 8H), 1.58–1.65 (m, 2H), 1.69–1.75 (m, 1H), 2.00–2.06 (m, 2H), 2.10–2.17 (m, 1H), 2.34 (t, $J = 7.4$ Hz, 2H), 2.41–2.51 (m, 2H), 2.94–3.00 (m, 1H), 5.32–5.45 (m, 2H), 6.18 (dd, $J = 5.8$, 1.7 Hz, 1H), 7.73 (dd, $J = 5.8$, 2.8 Hz, 1H). ^{13}C-NMR (100 MHz, $CDCl_3$): δ 14.0, 20.7, 23.7, 24.5, 27.5, 28.9, 29.0, 29.5, 30.7, 34.0, 44.3, 49.8, 126.9, 132.4, 133.0, 167.3, 179.8, 211.0. $[\alpha]_D^{20} = +8°$ [c 6.5, $CHCl_3$].

4: pale yellow oil, yield 18%, UPLC-UV/VIS RT, purity (min., %): 24.77, 91.0. ESI$^+$-MS *m/z* (rel. int. %, ion): 298.3 (100, $[M+H]^+$). ^{1}H-NMR (400 MHz, $CDCl_3$) δ (ppm): 1.10–1.18 (m, 1H), 1.31–1.35 (m, 8H), 1.59–1.64 (m, 2H), 1.69–1.77 (m, 1H), 2.09–2.18 (m, 1H), 2.35 (t, $J = 7.5$ Hz, 2H), 2.41–2.55 (m, 2H), 2.55–2.65 (m, 1H), 2.94–3.01 (m, 1H), 5.35 (dd, $J = 10.8$, 7.2, 5.4 Hz, 1H), 5.42 (bd, $J = 10.8$ Hz, 1H), 6.19 (dd, $J = 5.8$, 1.7 Hz, 1H), 7.75 (dd, $J = 5.8$, 2.8 Hz, 1H). ^{13}C-NMR (100 MHz, $CDCl_3$): δ 23.7, 24.6, 27.5, 28.9, 29.1, 29.5, 30.7, 33.8, 44.3, 49.8, 126.9, 132.4, 132.9, 167.4, 179.2, 211.1. HRMS (ESI-QTOF): *m/z* calc for $C_{18}H_{23}D_5O_3$ $[M+H]^+$ 298.2425, found 298.2427.

4.2.2. Synthesis of (isobutyl carbonic) 8-[(1S*,5S*)-4-oxo-5-((Z)-pent-2-en-1-yl)cyclopent-2-en-1-yl]octanoic anhydride (5) and (isobutyl carbonic) 8-[(1S*,5S*)-4-oxo-5-((Z)-pent-2-en-1-yl-4,4,5,5,5-d_5)cyclopent-2-en-1-yl]octanoic anhydride (6)

Isobutyl chloroformate (1.1 eq.) was dropwise added under Ar atmosphere to the solution of **3** or **4** (1 eq) and TEA (1.2 eq.) in dry THF (0.07 M) cooled to −10 °C. The resulting mixture was stirred at −10 °C for 30 min and then filtered using MicroSpin centrifugation filters (NYLON 0.2 μm, Chromservis). The filtrates were used immediately in the next step without any purification or characterization.

4.2.3. Silylation of amino acids - compounds 8a-g

Suspension of amino acid **7a-g** (3 eq.), TMS-Cl (typically 7.5 eq., for Asp (**7f**) and Glu (**7g**) 10.5 eq.), and TEA (12 eq.) in dry acetonitrile was refluxed under Ar atmosphere until complete dissolution of the starting amino acid. The resulting solution was cooled to room temperature and filtered using a MicroSpin centrifugation filter (NYLON 0.2 μm). Filtrate was used immediately in the next step without any purification or characterization.

4.2.4. Synthesis of amino acid conjugates of cis-OPDA and (17,17,18,18,18-d_5)-cis-OPDA – compounds 9a-g, 10a-g

The filtrate obtained in step 4.2.2 was under an inert atmosphere added to the solution of silylated amino acids solution in acetonitrile from step 4.2.3 cooled to 0 °C. The reaction mixture was stirred at 0 °C for 2 h. After acidification by 1 mol/l HCl to pH ~3, the mixture was diluted with water and extracted by $CHCl_3$ (4 × 5 ml). Combined organic layers were washed with brine, dried over Na_2SO_4, filtered, and evaporated under reduced pressure. Products were further purified using preparative LC. Fraction containing purified product were partially evaporated and extracted by $CHCl_3$. Combined organic layers were dried over Na_2SO_4, filtered, and evaporated under reduced pressure.

{8-[(1*S**,5*S**)-4-oxo-5-((*Z*)-pent-2-en-1-yl)cyclopent-2-en-1-yl]octanoyl}glycine **9a**: white solid, yield 52%, UPLC-PDA RT, purity (min., %): 22.61, 99.9. ESI$^+$-MS *m/z* (rel. int. %, ion): 350.4 (100, $[M+H]^+$). ^{1}H-NMR (400 MHz, $CDCl_3$) δ (ppm): 0.96 (t, $J = 7.4$ Hz, 3H), 1.13–1.17 (m, 1H), 1.27–1.40 (m, 8H), 1.59–1.72 (m, 3H), 2.01–2.17 (m, 3H), 2.26 (t, $J = 7.5$ Hz, 2H), 2.42–2.51 (m, 2H), 2.96–3.00 (m, 1H), 4.06 (d, $J = 5.0$ Hz, 2H), 5.34–5.45 (m, 2H), 6.19 (dd, $J = 5.8$, 1.7 Hz, 1H), 6.26 (t, $J = 5.0$ Hz, 1H), 7.75 (dd, $J = 5.9$, 2.7 Hz, 1H). ^{13}C-NMR (100 MHz, $CDCl_3$) δ (ppm): 14.0, 20.7, 23.7, 25.4, 27.5, 29.0, 29.1, 29.5, 30.7, 36.2, 41.4, 44.3, 49.9, 126.8, 132.3, 133.0, 167.6, 172.3, 174.3, 211.4. HRMS (ESI-QTOF): *m/z* calc for $C_{20}H_{31}NO_4$ $[M+H]^+$ 350.2326, found 350.2332.

{8-[(1*S**,5*S**)-4-oxo-5-((*Z*)-pent-2-en-1-yl)cyclopent-2-en-1-yl]octanoyl}-L-alanine **9b**: white solid, yield 58%, UPLC-UV/VIS RT, purity (min., %): 23.16, 99.9. ESI$^+$-MS *m/z* (rel. int. %, ion): 364.4 (100, $[M+H]^+$). ^{1}H-NMR (500 MHz, $CDCl_3$) δ (ppm): 0.96 (t, $J = 7.5$ Hz, 3H), 1.14–1.18 (m, 1H), 1.30 (s, 8H), 1.45 (d, $J = 7.3$ Hz, 3H), 1.62 (t, $J = 6.4$ Hz, 2H), 1.69–1.74 (m, 1H), 2.02–2.08 (m, 2H), 2.10–2.16 (m, 1H), 2.23 (t, $J = 7.5$ Hz, 2H), 2.42–2.51 (m, 2H), 2.98 (d, $J = 3.1$ Hz, 1H), 4.54–4.60 (m, 1H), 5.33–5.43 (m, 2H), 6.19 (dd, $J = 5.8$, 1.8 Hz, 1H), 6.22 (d, $J = 6.7$ Hz, 1H), 7.75 (dd, $J = 5.8$, 2.4 Hz, 1H). ^{13}C-NMR (125 MHz, $CDCl_3$) δ (ppm): 14.0, 18.1, 20.8, 23.7, 25.4, 27.5, 27.5, 29.0, 29.1, 29.5, 29.7, 30.7, 36.3, 44.3, 48.2, 49.9, 126.8, 132.4, 133.0, 167.5, 167.5, 173.7, 175.6, 211.3, 211.4. HRMS (ESI-QTOF): *m/z* calc for $C_{21}H_{33}NO_4$ $[M+H]^+$ 364.2482, found 364.2500.

{8-[(1*S**,5*S**)-4-oxo-5-((*Z*)-pent-2-en-1-yl)cyclopent-2-en-1-yl]octanoyl}-L-valine **9c**: white solid, yield 82%, UPLC-UV/VIS RT, purity (min., %): 24.57, 99.9. ESI$^+$-MS *m/z* (rel. int. %, ion): 392.5 (100, $[M+H]^+$). ^{1}H-NMR (400 MHz, $CDCl_3$) δ (ppm): 0.94 (t, $J = 6.8$ Hz, 3H), 0.96 (t, $J = 7.5$ Hz, 3H), 0.97 (t, $J = 6.8$ Hz, 3H), 1.11–1.19 (m, 1H), 1.35 (bs, 8H), 1.60–1.65 (m, 2H), 1.68–1.75 (m, 1H), 2.01–2.09 (m, 2H), 2.11–2.17 (m, 1H), 2.19–2.27 (m, 3H), 2.42–2.52 (m, 2H), 2.96–2.99 (m, 1H), 4.58 (dd, $J = 8.7$, 4.8 Hz, 1H), 5.32–5.45 (m, 2H), 6.06 (d, $J = 8.7$ Hz, 1H), 6.19 (dd, $J = 5.8$, 1.7 Hz, 1H), 7.74 (dd, $J = 5.7$, 2.7 Hz, 1H). ^{13}C-NMR (100 MHz, $CDCl_3$) δ (ppm): 14.0, 17.7, 19.0, 20.8, 23.7, 25.6, 27.5, 27.5, 29.0, 29.1, 29.6, 29.7, 30.7, 30.9, 36.6, 44.3, 49.9, 56.9, 126.9, 132.4, 133.0, 167.5, 167.5, 173.8, 175.1, 211.3, 211.4. HRMS (ESI-QTOF): *m/z* calc for $C_{23}H_{37}NO_4$ $[M+H]^+$ 392.2795, found 392.2806.

{8-[(1*S**,5*S**)-4-oxo-5-((*Z*)-pent-2-en-1-yl)cyclopent-2-en-1-yl]octanoyl}-L-isoleucine **9d**: white solid, yield 62%, UPLC-UV/VIS RT, purity (min., %): 25.31, 99.3. ESI$^+$-MS *m/z* (rel. int. %, ion): 406.6 (100, $[M+H]^+$). ^{1}H-NMR (500 MHz, $CDCl_3$) δ (ppm): 0.90–0.98 (m, 9H), 1.14–1.38 (m, 10H), 1.46–1.52 (m, 1H), 1.60–1.74 (m, 3H), 1.92–1.97 (m, 1H), 2.02–2.08 (m, 2H), 2.10–2.16 (m, 1H), 2.24 (t, $J = 7.5$ Hz, 2H), 2.42–2.51 (m, 2H), 2.96–2.98 (m, 1H), 4.61 (dd, $J = 8.6$, 4.9 Hz, 1H), 5.33–5.44 (m, 2H), 6.09 (d, $J = 8.6$ Hz, 1H), 6.19 (dd, $J = 6.0$, 1.7 Hz, 1H), 7.74 (dd, $J = 5.8$, 2.7 Hz, 1H). ^{13}C-NMR (125 MHz, $CDCl_3$) δ (ppm): 11.6, 14.0, 15.4, 20.8, 23.7, 25.1, 25.6, 27.5, 27.5, 29.0, 29.1, 29.1, 29.6, 30.7, 36.5, 37.6, 44.3, 49.9, 56.3, 126.9, 132.4, 133.0, 167.5, 167.5, 173.6, 175.1, 175.1, 211.3, 211.4. HRMS (ESI-QTOF): *m/z* calc for $C_{24}H_{39}NO_4$ $[M+H]^+$ 406.2952, found 406.2962.

{8-[(1*S**,5*S**)-4-oxo-5-((*Z*)-pent-2-en-1-yl)cyclopent-2-en-1-yl]octanoyl}-L-phenylalanine **9e**: white solid, yield 48%, UPLC-UV/VIS RT, purity (min., %): 25.29, 99.9. ESI$^+$-MS *m/z* (rel. int. %, ion): 440.5 (100, $[M+H]^+$). ^{1}H-NMR (500 MHz, $CDCl_3$) δ (ppm): 0.96 (t, $J = 7.6$ Hz, 3H), 1.13–1.15 (m, 1H), 1.25–1.31 (m, 7H), 1.28–1.38 (m, 1H), 1.53–1.59 (m, 2H), 1.68–1.75 (m, 1H), 2.02–2.08 (m, 2H), 2.10–2.15 (m, 1H), 2.17 (t, $J = 7.5$ Hz, 2H), 2.43–2.51 (m, 2H), 2.96–2.98 (m, 1H), 3.12 (dd, $J = 14.1$, 6.4 Hz, 1H), 3.23 (dd, $J = 14.1$, 5.8 Hz, 1H), 4.88 (dt, $J = 7.4$, 6.0 Hz, 1H), 5.33–5.45 (m, 2H), 6.01 (d, $J = 7.3$ Hz, 1H), 6.18 (dd, $J = 5.8$, 1.8 Hz, 1H), 7.15–7.16 (m, 2H), 7.22–7.30 (m, 3H), 7.74 (dd, $J = 5.7$, 2.3 Hz, 1H). ^{13}C-NMR (125 MHz, $CDCl_3$) δ (ppm): 14.0, 20.8, 23.7, 25.4, 27.5, 27.5, 29.0, 29.0, 29.1, 29.5, 29.7, 30.7, 36.3, 37.2, 44.3, 49.9, 53.0, 126.8, 127.1, 128.6, 129.3, 132.4, 133.0, 135.7, 167.5, 167.6, 173.7, 174.1, 211.4, 211.4. HRMS (ESI-QTOF): *m/z* calc for $C_{27}H_{37}NO_4$ $[M+H]^+$ 440.2795, found 440.2794.

{8-[(1*S**,5*S**)-4-oxo-5-((*Z*)-pent-2-en-1-yl)cyclopent-2-en-1-yl]octanoyl}-L-aspartic acid **9f**: white solid, yield 55%, UPLC-UV/VIS RT,

purity (min., %): 22.13, 99.9. ESI$^+$-MS *m/z* (rel. int. %, ion): 408.5 (100, [M+H]$^+$). ^{1}H-NMR (400 MHz, $CDCl_3$) δ (ppm): 0.95 (t, *J* = 7.5 Hz, 3H), 1.15–1.20 (m, 1H), 1.24–1.28 (m, 8H), 1.59–1.71 (m, 3H), 2.01–2.16 (m, 3H), 2.25 (bt, *J* = 6.6 Hz, 2H), 2.43–2.51 (m, 2H), 2.85–3.07 (m, 3H), 4.87 (bs, 1H), 5.31–5.45 (m, 2H), 6.20 (d, *J* = 5.5 Hz, 1H), 7.01 (d, *J* = 6.6 Hz, 1H), 7.77 (dd, *J* = 5.5, 2.3 Hz, 1H), 9.30 (bs, 2H). ^{13}C-NMR (100 MHz, $CDCl_3$) δ (ppm): 14.0, 20.6, 20.8, 23.7, 25.4, 27.3, 28.9, 29.1, 29.5, 30.6, 36.1, 44.3, 48.5, 50.0, 126.7, 132.3, 133.1, 168.0, 174.2, 174.5, 174.9, 211.9, 211.9. HRMS (ESI-QTOF): *m/z* calc for $C_{22}H_{33}NO_6$ [M+H]$^+$ 408.2381, found 408.2386.

{8-[(1*S**,5*S**)-4-oxo-5-((*Z*)-pent-2-en-1-yl)cyclopent-2-en-1-yl]octanoyl}-L-glutamic acid **9g**: White solid, yield 73%, UPLC-UV/VIS RT, purity (min., %): 22.19, 99.0. ESI$^+$-MS *m/z* (rel. int. %, ion): 422.5 (100, [M+H]$^+$). ^{1}H-NMR (500 MHz, $CDCl_3$) δ (ppm): 0.96 (t, *J* = 7.6 Hz, 3H), 1.12–1.21 (m, 1H), 1.30–1.38 (m, 8H), 1.58–1.62 (m, 2H), 1.69–1.74 (m, 1H), 2.00–2.07 (m, 3H), 2.11–2.16 (m, 1H), 2.22–2.27 (m, 3H), 2.43–2.50 (m, 4H), 2.97–3.01 (m, 1H), 4.62 (bq, *J* = 6.2 Hz, 1H), 5.32–5.44 (m, 2H), 6.19 (dd, *J* = 5.8, 1.5 Hz, 1H), 6.79 (d, *J* = 7.0 Hz, 1H), 7.77 (dd, *J* = 5.8, 2.5 Hz, 1H), 8.79 (bs, 2H). ^{13}C-NMR (125 MHz, $CDCl_3$) δ (ppm): 14.0, 20.8, 23.7, 25.5, 26.8, 27.4, 29.0, 29.1, 29.5, 29.9, 30.7, 36.2, 44.3, 49.9, 51.6, 126.8, 132.3, 133.1, 167.9, 174.5, 177.5, 211.8. HRMS (ESI-QTOF): *m/z* calc for $C_{23}H_{35}NO_6$ [M+H]$^+$ 422.2537, found 422.2533.

{8-[(1*S**,5*S**)-4-oxo-*5*-((Z)-pent-2-en-1-yl-4,4,5,5,5-d_5)cyclopent-2-en-1-yl]octanoyl}glycine **10a**: white solid, yield 51%, UPLC-UV/VIS RT, purity (min., %): 22.57, 99.9. ESI$^+$-MS *m/z* (rel. int. %, ion): 355.4 (100, [M+H]$^+$). ^{1}H-NMR (500 MHz, $CDCl_3$) δ (ppm): 1.15–1.17 (m, 1H), 1.30–1.40 (m, 9H), 1.60–1.65 (m, 2H), 1.70–1.75 (m, 1H), 2.11–2.16 (m, 1H), 2.26 (t, *J* = 7.5 Hz, 2H), 2.43–2.51 (m, 2H), 2.96–3.01 (m, 1H), 4.07 (d, *J* = 5.2 Hz, 2H), 5.33–5.38 (m, 1H), 5.42 (bd, *J* = 11.0 Hz, 1H), 6.17 (t, *J* = 4.9 Hz, 1H), 6.19 (dd, *J* = 5.8, 1.8 Hz, 1H), 7.75 (dd, *J* = 5.8, 2.8 Hz, 1H). ^{13}C-NMR (125 MHz, $CDCl_3$) δ (ppm): 13.1, 23.7, 25.4, 27.5, 29.0, 29.1, 29.5, 30.7, 36.2, 41.4, 44.3, 49.9, 126.9, 132.4, 132.9, 167.5, 174.2, 211.3. HRMS (ESI-QTOF): *m/z* calc for $C_{20}H_{26}D_5NO_4$ [M+H]$^+$ 355.2640, found 355.2648.

{8-[(1*S**,5*S**)-4-oxo-*5*-((Z)-pent-2-en-1-yl-4,4,5,5,5-d_5)cyclopent-2-en-1-yl]octanoyl}-L-alanine **10b**: white solid, yield 43%, UPLC-UV/VIS RT, purity (min., %): 23.17, 99.9. ESI$^+$-MS *m/z* (rel. int. %, ion): 369.5 (100, [M+H]$^+$). ^{1}H-NMR (500 MHz, $CDCl_3$) δ (ppm): 1.27–1.31 (m, 8H), 1.46 (d, *J* = 7.3 Hz, 3H), 1.60–1.75 (m, 4H), 2.10–2.16 (m, 1H), 2.23 (t, *J* = 7.5 Hz, 2H), 2.30–2.36 (m, 1H), 2.42–2.47 (m, 1H), 2.48–2.54 (m, 1H), 2.96–3.01 (m, 1H), 4.57 (pent., *J* = 7.0 Hz, 1H), 5.34–5.39 (m, 1H), 5.42 (d, *J* = 10.7 Hz, 1H), 6.04 (d, *J* = 6.4 Hz, 1H), 6.19 (dd, *J* = 5.8, 1.8 Hz, 1H), 7.74 (dd, *J* = 5.8, 2.8 Hz, 1H). HRMS (ESI-QTOF): *m/z* calc for $C_{21}H_{28}D_5NO_4$ [M+H]$^+$ 369.2796, found 369.2802.

{8-[(1*S**,5*S**)-4-oxo-*5*-((Z)-pent-2-en-1-yl-4,4,5,5,5-d_5)cyclopent-2-en-1-yl]octanoyl}-L-valine **10c**: white solid, yield 51%, UPLC-UV/VIS RT, purity (min., %): 24.55, 99.9. ESI$^+$-MS *m/z* (rel. int. %, ion): 397.5 (100, [M+H]$^+$). ^{1}H-NMR (500 MHz, $CDCl_3$) δ (ppm): 0.95 (d, *J* = 6.7 Hz, 3H), 0.99 (d, *J* = 6.7 Hz, 3H), 1.13–1.22 (m, 1H), 1.27–1.40 (m, 8H), 1.60–1.75 (m, 3H), 2.10–2.16 (m, 1H), 2.22–2.23 (m, 1H), 2.25 (t, *J* = 7.6 Hz, 2H), 2.30–2.35 (m, 1H), 2.43–2.47 (m, 1H), 2.49–2.52 (m, 1H), 2.97–3.00 (m, 1H), 4.57 (dd, *J* = 8.6, 4.9 Hz, 1H), 5.34–5.38 (m, 1H), 5.42 (d, *J* = 11.0 Hz, 1H), 5.97 (d, *J* = 8.6 Hz, 1H), 6.19 (dd, *J* = 5.8, 1.8 Hz, 1H), 7.74 (dd, *J* = 5.8, 2.8 Hz, 1H) . ^{13}C-NMR (125 MHz, $CDCl_3$) δ (ppm): 17.7, 19.0, 23.7, 23.7, 25.6, 27.4, 27.5, 29.0, 29.0, 29.2, 29.6, 29.7, 30.7, 30.8, 36.6, 44.3, 49.9, 49.9, 126.9, 132.4, 132.4, 132.9, 167.3, 167.4, 173.7, 211.2, 211.3. HRMS (ESI-QTOF): *m/z* calc for $C_{23}H_{32}D_5NO_4$ [M+H]$^+$ 397.3109, found 397.3118.

{8-[(1*S**,5*S**)-4-oxo-*5*-((Z)-pent-2-en-1-yl-4,4,5,5,5-d_5)cyclopent-2-en-1-yl]octanoyl}-L-isoleucine **10d**: white solid, yield 23%, UPLC-UV/VIS RT, purity (min., %): 25.27, 98.3. ESI$^+$-MS *m/z* (rel. int. %, ion): 411.6, (100, [M+H]$^+$). ^{1}H-NMR (400 MHz, $CDCl_3$) δ (ppm): 0.92–0.96 (m, 6H), 1.14–1.22 (m, 1H), 1.27–1.39 (m, 8H), 1.47–1.52 (m, 1H), 1.60–1.72 (m, 3H), 1.92–1.97 (m, 1H), 2.09–2.17 (m, 1H), 2.24 (t, *J* = 7.5 Hz, 2H), 2.42–2.52 (m, 2H), 2.98 (d, *J* = 3.2 Hz, 1H), 3.64–3.66 (m, 1H), 4.61 (dd, *J* = 8.5, 4.8 Hz, 1H), 5.34–5.39 (m, 1H), 5.42 (d, *J* = 11.0 Hz, 1H), 6.02 (d, *J* = 8.5 Hz, 1H), 6.19 (dd, *J* = 5.8, 1.7 Hz, 1H), 7.74 (dd, *J* = 5.7, 2.7 Hz, 1H). ^{13}C-NMR (100 MHz, $CDCl_3$) δ (ppm): 11.6, 14.1, 15.4, 23.7, 25.1, 25.6, 26.7, 27.0, 27.4, 27.5, 29.0, 29.0, 29.1, 29.6, 29.7, 30.7, 36.6, 37.5, 44.3, 49.9, 56.3, 126.9, 132.4, 132.9, 167.4, 167.5, 173.5, 174.8, 174.9, 176.4, 177.0, 211.2, 211.3. HRMS (ESI-QTOF): *m/z* calc for $C_{24}H_{34}D_5NO_4$ [M+H]$^+$ 411.3266, found 411.3272.

{8-[(1*S**,5*S**)-4-oxo-*5*-((Z)-pent-2-en-1-yl-4,4,5,5,5-d_5)cyclopent-2-en-1-yl]octanoyl}-L-phenylalanine **10e**: white solid, yield 63%, UPLC-UV/VIS RT, purity (min., %): 25.28, 99.9. ESI$^+$-MS *m/z* (rel. int. %, ion): 445.5 (100, [M+H]$^+$). ^{1}H-NMR (500 MHz, $CDCl_3$) δ (ppm): 1.25–1.32 (m, 8H), 1.55–1.72 (m, 3H), 2.10–2.14 (m, 1H), 2.17 (t, *J* = 7.5 Hz, 2H), 2.29–2.36 (m, 1H), 2.43–2.47 (m, 1H), 2.48–2.52 (m, 1H), 2.96–3.00 (m, 1H), 3.13 (dd, *J* = 14.1, 6.1 Hz, 1H), 3.24 (dd, *J* = 14.1, 5.5 Hz, 1H), 4.87 (q, *J* = 6.4 Hz, 1H), 5.35–5.38 (m, 1H), 5.42 (d, *J* = 11.0 Hz, 1H), 5.92 (d, *J* = 7.3 Hz, 1H), 6.18 (dd, *J* = 5.8, 1.8 Hz, 1H), 7.15–7.17 (m, 2H), 7.25–7.31 (m, 3H), 7.74 (dd, *J* = 5.8, 2.5 Hz, 1H). ^{13}C-NMR (125 MHz, $CDCl_3$) δ (ppm): 23.7, 25.4, 27.5, 27.5, 28.9, 29.1, 29.5, 29.7, 30.7, 36.4, 37.2, 44.3, 49.9, 126.9, 127.2, 128.6, 129.3, 132.4, 132.9, 135.7, 167.4, 167.4, 173.6, 211.2, 211.3. HRMS (ESI-QTOF): *m/z* calc for $C_{27}H_{32}D_5NO_4$ [M+H]$^+$ 445.3109, found 445.3113.

{8-[(1*S**,5*S**)-4-oxo-*5*-((Z)-pent-2-en-1-yl-4,4,5,5,5-d_5)cyclopent-2-en-1-yl]octanoyl}-L-aspartic acid **10f**: white solid, yield 63%, UPLC-UV/VIS RT, purity (min., %): 22.13, 99.9. ESI$^+$-MS *m/z* (rel. int. %, ion): 413.5 (100, [M+H]$^+$). ^{1}H-NMR (500 MHz, $CDCl_3$) δ (ppm): 1.13–1.20 (m, 1H), 1.29–1.42 (m, 9H), 1.60 (bs, 2H), 1.70–1.74 (m, 1H), 2.09–2.15 (m, 1H), 2.25 (t, *J* = 7.0 Hz, 2H), 2.44–2.51 (m, 2H), 2.88–3.06 (m, 3H), 4.85 (bs, 1H), 5.32–5.37 (m, 1H), 5.41 (d, *J* = 10.7 Hz, 1H), 6.20 (dd, *J* = 5.8, 1.2 Hz, 1H), 7.00 (bs, 1H), 7.77 (dd, *J* = 5.6, 2.5 Hz, 1H). ^{13}C-NMR (125 MHz, $CDCl_3$) δ (ppm): 23.7, 25.4, 27.3, 28.9, 29.0, 29.5, 29.7, 30.6, 36.1, 44.3, 50.0, 126.8, 132.3, 133.0, 168.0, 168.1, 174.4, 211.9, 212.0. HRMS (ESI-QTOF): *m/z* calc for $C_{22}H_{28}D_5NO_6$ [M+H]$^+$ 413.2694, found 413.2697.

{8-[(1*S**,5*S**)-4-oxo-*5*-((Z)-pent-2-en-1-yl-4,4,5,5,5-d_5)cyclopent-2-en-1-yl]octanoyl}-L-glutamic acid **10g**: white solid, yield 70%, UPLC-UV/VIS RT, purity (min., %): 22.17, 99.9. ESI$^+$-MS *m/z* (rel. int. %, ion): 427.5 (100, [M+H]$^+$). ^{1}H-NMR (500 MHz, $CDCl_3$) δ (ppm): 1.14–1.19 (m, 1H), 1.26–1.37 (m, 9H), 1.59–1.71 (m, 3H), 2.05–2.15 (m, 2H), 2.21–2.26 (m, 3H), 2.43–2.51 (m, 4H), 2.96–3.00 (m, 1H), 4.62 (q, *J* = 6.7 Hz, 1H), 5.32–5.37 (m, 1H), 5.40 (d, *J* = 11.0 Hz, 1H), 6.19 (dd, *J* = 5.8, 1.5 Hz, 1H), 6.76 (d, *J* = 7.3 Hz, 1H), 7.76 (dd, *J* = 5.8, 2.7 Hz, 1H) . ^{13}C-NMR (125 MHz, $CDCl_3$) δ (ppm): 23.7, 25.4, 26.8, 27.4, 28.9, 29.1, 29.5, 29.9, 30.7, 36.2, 44.3, 49.9, 126.8, 132.3, 133.0, 167.9, 174.5, 177.4, 211.7, 211.8. HRMS (ESI-QTOF): *m/z* calc for $C_{23}H_{30}D_5NO_6$ [M+H]$^+$ 427.2851, found 427.2845.

4.3. Chemicals

Analytical standards and deuterium-labeled ISs of OPDA-aa (Table 1) were obtained by organic synthesis described above in section 4.1. and 4.2. The weighted standard amounts were dissolved in acetonitrile to an exact concentration of around 2 mg/ml. Each was further diluted in acetonitrile to obtain individual stock solutions of concentration 10^{-3} mol/l. A mixed solution of standards was prepared in 20% acetonitrile at a concentration of 10^{-6} mol/l to be used in validation experiments and preparation of calibration standards. The mix of deuterated IS was prepared equally. All standard solutions were stored at −20 °*C*. Solvents and chemicals for sample preparation and chromatography (methanol, acetonitrile, ammonium hydroxide, acetic, formic, and hydrochloric acid) were purchased from Sigma-Aldrich (St. Luis, MO, USA). All aq. solutions were prepared freshly from Milli-Q water obtained by purifying demineralized water in a Simplicity 185 System.

4.4. Plant material

The *Arabidopsis thaliana* (*At*) ecotype Col-0 plants were cultivated for

30 days, in the soil in a growth chamber under a short-day photoperiod (16 h dark at 18 °C, 8 h light at 22 °C) with a light intensity 100 μE m^{-2} s^{-1}. After 30 days the leaves were harvested for method optimization and validation. For the wounding experiment, four leaves of each 30-day-old plant were mechanically stressed by pinching with serrated-tip laboratory forceps at three places of the leaf. The whole stressed leaves were harvested at 6 time points: 5, 15, 30, 60, and 180 min after wounding. For each time point, four individual plants were used. The time point 0 min represents not wounded leaves from individual plants collected before the wounding started. The harvested plant tissue was immediately frozen in liquid nitrogen and stored at 80 °C until extraction and purification.

4.5. Procedures during sample preparation optimization

To assess the pH stability, the mixed solution of standard (5 pmol) was incubated in 1 ml of 2% formic acid in methanol, 5% ammonium hydroxide in methanol or methanol *for* 30 min, evaporated to dryness *in vacuo* by Centrivap concentrator (Labconco, Kansas City, MO, USA), dissolved in 50 μl of 20% acetonitrile in water and injected. The stability was calculated as the average peak areas of OPDA-aa in acidic or alkaline samples divided by peak areas of samples in methanol, expressed as a percentage.

For SPE optimization, generic protocols from the manufacturer (Waters) were adopted. The Oasis® HLB 1 cc 30 mg columns (Waters, Milford, MA, USA) were activated by 2 ml of methanol and 1 ml of water, 1 ml of 10% methanol spiked with 1 pmol of analytes was loaded, washed with 1 ml of water and the analytes were eluted with 3 ml of 80% aq. methanol. The Oasis® MAX 1 cc 30 mg columns (Waters, Milford, MA, USA) were activated by 2 ml of methanol and 1 ml of water, 1 ml of 1% formic acid in 10% aq. methanol spiked with 1 pmol of analytes was loaded, washed with 1 ml of 5% ammonium hydroxide in water and the analytes were eluted with 2 ml of methanol and 3 ml of 2% formic acid in methanol. The purification recoveries were calculated as the mean area of OPDA-aa processed by MAX or HLB divided by the peak area of OPDA-aa without SPE, expressed as a percentage.

The impact of methanol content in the extraction solution and the acidification step during the purification experiments were performed following the general protocol described for the HLB columns above. Only the condition optimized was modified.

4.6. Sample preparation protocol

The frozen plant material was homogenized with mortar and pestle under liquid nitrogen to a fine green powder. Approximately 10 mg of fr. wt samples were weighed into 2 ml safe-lock Eppendorf tubes. To extract the samples, 1 ml of ice-cold 10% methanol in water, 4 ceria-stabilized zirconium oxide 2 mm beads (Retsch GmbH, Haan, Germany), and 5 pmols of IS (5 μl of 10^{-6} mol/l mixed IS solution) was added into each sample. The samples were placed on an MM 400 mixer mill (Retsch GmbH, Haan, Germany) (29 Hz, 10 min, precooled holders) and centrifuged (25 800 g, 20 min, 8 °C). The supernatants were loaded on SPE Oasis® HLB 1 cc 30 mg columns (Waters, Milford, MA, USA), as described in (Floková et al., 2014). Shortly, the SPE columns were activated by 2 ml of methanol and 1 ml of 0.1% formic acid in water, respectively. After loading the extracts, the SPE columns were washed with 10% methanol in water, and the analytes were eluted with 3 ml of 80% aq. methanol. The eluted fractions were evaporated to dryness *in vacuo* by Centrivap concentrator (Labconco, Kansas City, MO, USA) and stored at −20 °*C* until the analysis day.

4.7. LC-MS/MS analysis

All samples were analyzed on an Agilent 6490 Triple Quadrupole LC/MS system coupled to a 1290 Infinity LC system (Agilent Technologies, Santa Clara, CA, USA) using a chromatographic gradient reported in (Široká et al., 2022) in order to obtain the overall acidic phytohormone profiles (abscisates, auxins, JAs and salicylic acid) simultaneously with OPDA-aa conjugates levels. Before analysis, the evaporated samples were dissolved in 40 μl of 20% acetonitrile in water and 10 μl of each sample was injected onto an inlet filter-protected Kinetex Evo C18 reverse phase column (2.1 × 150 mm, particle size 2.6 μm; Phenomenex, Torrance, CA, USA) maintained at 50 °C. The mobile phases consisted of 10 mmol/l formic acid in water and methanol, and gradient elution at a 0.3 ml/min flow rate was applied. The chromatography started with 2 min of 20% methanol followed by 11.5 min long gradient from 20 to 90% of methanol, continuing within 0.5 min from 90 to 100%. The 100% methanol was kept for 1 min, and within next 0.5 min, the methanol dropped to initial conditions, 20% methanol, which was maintained for another 3 min before a new injection.

The MS system was operated in dynamic multiple reaction monitoring mode in positive and negative electrospray ionization mode. The multiple reactions monitoring transitions and collision energies were optimized on standards. The nozzle voltage was set to 0 V, the capillary voltage to 2800/3000 V positive/negative mode, and the drying gas was at 130 °C with a flow rate of 14 l/min. The sheath gas was heated to 400 °C, and its flow rate was 12 l/min. The MassHunter Quantitative software package version B.09.00 (Agilent Technologies, Santa Clara, CA, USA) was used for data processing.

4.8. Method validation

The validation experiments were performed using 10 mg fr. wt of 30-day-old *At* leaves following the Sample preparation protocol (4.6.). Accuracy and precision were evaluated by spiking the plant material at three concentration levels (0.05, 0.5, and 5 pmols) in four replicates. Accuracy was assessed by determining analyte levels (pmol) in spiked samples with endogenous levels subtracted and linked to the spike's nominal amount (pmol), expressed as the percentage of the spike. Precision was assessed as the relative standard deviation (%) of analyte levels in spiked samples. The RE, PE, and ME were assessed following (Matuszewski et al., 2003) spiking the plant material at a single concentration level (5 pmol) before (A) or after (B) purification in four replicates and simultaneous analysis of a neat solution (C). Specifically, RE = A/B x 100 (%), PE = A/C x 100 (%), and ME = B/C x 100 (%), where (A) represents the mean peak area of analytes in samples spiked before purification with endogenous levels subtracted, (B) represents the mean peak area of analytes in samples spiked after purification with endogenous levels subtracted and (C) represents the mean peak area of analytes in neat standard solution not undergoing sample preparation corresponding to the amount of the spike.

4.9. Identification and quantification

For confirmation of the identity of analytes, the guidelines of the World Anti-doping Agency were adopted (WADA Technical document TD2023IDCR). To evaluate the chromatographic criteria, the RRt was calculated as the ratio of the Rt of the analyte to the Rt of the IS. Since the ISs were the stable isotope-labeled analogs of the analytes, the RRt shall not be different by more than 0.5% between the samples and a reference material (calibration curve) analyzed in the same batch. Based on the fragmentation spectra of the analytes (Supplemental Figs. S1–S7), the most abundant ions typical for the structure were chosen to be the diagnostic ions. For MS identification, two diagnostic MRM transitions shall be acquired. Their RAs were calculated by dividing the peak area of the MRM transition of the lower abundance by the peak area of the most abundant MRM – the reference diagnostic MRM (see Table 1 or marked as "R" in Supplementa1 Figs. S13-S15), expressed as the percentage. Based on the RAs in reference material (calibration curve), the tolerance windows for RA in samples were applied: RA 50–100% in reference material allows ± 10% (absolute) tolerance window of RA in samples, RA 25–50% in reference material allows ± 20% (relative to estimated

RA) tolerance window of RA in samples, and RA 1–25% in reference material allows ± 5% (absolute) tolerance window of RA in samples.

The limit of detection (LOD) was defined as three times the noise height. The LODs were determined from calibration curves constructed by plotting the peak height of the analyte in calibration standards providing linear signal (0.005–5 pmols) and the corresponding amount of substance injected. The limit of quantification (LOQ) was set as the lowest amount of substance (pmol) in the calibration curve linear range. For LOQs, see the linear range of the method in Table 1. The signal corresponding to LOQ was ten times the noise height or more for all analytes.

The content of the analytes in the samples was estimated based on calibration curves ranging over five orders of magnitude and analyzed in the same analytical batch with samples. The calibration curves were constructed by plotting the known concentration of the calibration standards on the "x" axis. The response was calculated as the ratio of the peak area of a standard and the peak area of IS multiplied by IS concentration on the "y" axis, both logarithmically transformed.

Declaration of competing interest

The authors declare that they have no known competing financial interests or personal relationships that could have appeared to influence the work reported in this paper.

Data availability

Data will be made available on request.

Acknowledgments

The authors thank Hana Svobodová, Miroslava Špičáková, Jaroslava Balonová, and Hana Omámiková for excellent technical support. The expert's opinion of Dr. Monika Židková Ph.D. is gratefully acknowledged. The work was financially supported by the Czech Science Foundation [grant number 19-10464Y] and by the EU Horizon-2020 project ADAPT [grant number 862858].

Appendix A. Supplementary data

Supplementary data to this article can be found online at https://doi.org/10.1016/j.phytochem.2023.113855.

References

Ainai, T., Matsuumi, M., Kobayashi, Y., 2003. Efficient total synthesis of 12-oxo-PDA and OPC-8:0. J. Org. Chem. 68, 7825–7832. https://doi.org/10.1021/jo0348571.

Aleman, G.H.J., Thirumalaikumar, V.P., Jander, G., Fernie, A.R., Skirycz, A., 2022. OPDA, more than just a jasmonate precursor. Phytochemistry 204, 113432. https://doi.org/10.1016/j.phytochem.2022.113432.

Arnold, M.D., Gruber, C., Floková, K., Miersch, O., Strnad, M., Novák, O., Wasternack, C., Hause, B., 2016. The recently identified isoleucine conjugate of *cis*-12-oxo-phytodienoic acid is partially active in *cis*-12-oxo-phytodienoic acid-specific gene expression of *Arabidopsis thaliana*. PLoS One 11, e0162829. https://doi.org/10.1371/journal.pone.0162829.

Bittner, A., Cieśla, A., Gruden, K., Lukan, T., Mahmud, S., Teige, M., Vothknecht, U.C., Wurzinger, B., 2022. Organelles and phytohormones: a network of interactions in plant stress responses. J. Exp. Bot. 73, 7165–7181. https://doi.org/10.1093/jxb/erac384.

Brunoni, F., Collani, S., Casanova-Sáez, R., Šimura, J., Karady, M., Schmid, M., Ljung, K., Bellini, C., 2020. Conifers exhibit a characteristic inactivation of auxin to maintain tissue homeostasis. New Phytol. 226, 1753–1765. https://doi.org/10.1111/nph.16463.

Brunoni, F., Pěnčík, A., Žukauskaitė, A., Ament, A., Kopečná, M., Collani, S., Kopečný, D., Novák, O., 2023. Amino acid conjugation of oxIAA is a secondary metabolic regulation involved in auxin homeostasis. New Phytol. 238, 2264–2270. https://doi.org/10.1111/nph.18887.

Cai, W.-J., Yu, L., Wang, W., Sun, M.-X., Feng, Y.-Q., 2019. Simultaneous determination of multiclass phytohormones in submilligram plant samples by one-pot multifunctional derivatization-assisted liquid chromatography–tandem mass spectrometry. Anal. Chem. 91, 3492–3499. https://doi.org/10.1021/acs.analchem.8b05087.

Chang, Y., Shi, M., Sun, Y., Cheng, H., Ou, X., Zhao, Y., Zhang, X., Day, B., Miao, C., Jiang, K., 2023. Light-induced stomatal opening in Arabidopsis is negatively regulated by chloroplast-originated OPDA signaling. Curr. Biol. 33, 1071–1081. https://doi.org/10.1016/j.cub.2023.02.012.

Chini, A., Fonseca, S., Fernandez, G., Adie, B., Chico, J.M., Lorenzo, O., Garcia-Casado, G., Lopez-Vidriero, I., Lozano, F.M., Ponce, M.R., Micol, J.L., Solano, R., 2007. The JAZ family of repressors is the missing link in jasmonate signalling. Nature 448, 666–671. https://doi.org/10.1038/nature06006.

Chini, A., Gimenez-Ibanez, S., Goossens, A., Solano, R., 2016. Redundancy and specificity in jasmonate signalling. Curr. Opin. Plant Biol. 33, 147–156. https://doi.org/10.1016/j.pbi.2016.07.005.

Chini, A., Monte, I., Zamarreño, A.M., García-Mina, J.M., Solano, R., 2023. Evolution of the jasmonate ligands and their biosynthetic pathways. New Phytol. 238, 2236–2246. https://doi.org/10.1111/nph.18891.

Chini, A., Monte, I., Zamarreño, A.M., Hamberg, M., Lassueur, S., Reymond, P., Weiss, S., Stintzi, A., Schaller, A., Porzel, A., García-Mina, J.M., Solano, R., 2018. An OPR3-independent pathway uses 4,5-didehydrojasmonate for jasmonate synthesis. Nat. Chem. Biol. 14, 171–178. https://doi.org/10.1038/nchembio.2540.

Davoine, C., Falletti, O., Douki, T., Iacazio, G., Ennar, N., Montillet, J.L., Triantaphylidès, C., 2006. Adducts of oxylipin electrophiles to glutathione reflect a 13 specificity of the downstream lipoxygenase pathway in the tobacco hypersensitive response. Plant Physiol. 140, 1484–1493. https://doi.org/10.1104/pp.105.074690.

Delfin, J.C., Kanno, Y., Seo, M., Kitaoka, N., Matsuura, H., Tohge, T., Shimizu, T., 2022. AtGH3.10 is another jasmonic acid-amido synthetase in Arabidopsis thaliana. Plant J. 110, 1082–1096. https://doi.org/10.1111/tpj.15724.

Floková, K., Feussner, K., Herrfurth, C., Miersch, O., Mik, V., Tarkowská, D., Strnad, M., Feussner, I., Wasternack, C., Novák, O., 2016. A previously undescribed jasmonate compound in flowering *Arabidopsis thaliana* - the identification of *cis*-(+)-OPDA-Ile. Phytochemistry 122, 230–237. https://doi.org/10.1016/j.phytochem.2015.11.012.

Floková, K., Tarkowská, D., Miersch, O., Strnad, M., Wasternack, C., Novák, O., 2014. UHPLC-MS/MS based target profiling of stress-induced phytohormones. Phytochemistry 105, 147–157. https://doi.org/10.1016/j.phytochem.2014.05.015.

Fonseca, S., Chini, A., Hamberg, M., Adie, B., Porzel, A., Kramell, R., Miersch, O., Wasternack, C., Solano, R., 2009. (+)-7-*iso*-Jasmonoyl-L-isoleucine is the endogenous bioactive jasmonate. Nat. Chem. Biol. 5, 344–350. https://doi.org/10.1038/nchembio.161.

Furey, A., Moriarty, M., Bane, V., Kinsella, B., Lehane, M., 2013. Ion suppression; A critical review on causes, evaluation, prevention and applications. Talanta 115, 104–122. https://doi.org/10.1016/j.talanta.2013.03.048.

Genva, M., Akong, F.O., Andersson, M.X., Deleu, M., Lins, L., Fauconnier, M.L., 2019. New insights into the biosynthesis of esterified oxylipins and their involvement in plant defense and developmental mechanisms. Phytochemistry Rev. 18, 343–358. https://doi.org/10.1007/s11101-018-9595-8.

Grieco, P.A., Abood, N., 1989. Cycloalkenone synthesis via Lewis acid-catalyzed retro Diels-Alder reactions of norbornene derivatives: synthesis of 12-oxophytodienoic acid (12-oxoPDA). J. Org. Chem. 54, 6008–6010. https://doi.org/10.1021/jo00287a005.

Hasanuzzaman, M., Nahar, K., Anee, T.I., Fujita, M., 2017. Glutathione in plants: biosynthesis and physiological role in environmental stress tolerance. Physiol. Mol. Biol. Plants 23, 249–268. https://doi.org/10.1007/s12298-017-0422-2.

Howe, G.A., Major, I.T., Koo, A.J., 2018. Modularity in jasmonate signaling for multistress resilience. Annu. Rev. Plant Biol. 69, 387–415. https://doi.org/10.1146/annurev-arplant-042817-040047.

Jez, J.M., 2022. Connecting primary and specialized metabolism: amino acid conjugation of phytohormones by GRETCHEN HAGEN 3 (GH3) acyl acid amido synthetases. Curr. Opin. Plant Biol. 66, 102194 https://doi.org/10.1016/j.pbi.2022.102194.

Kajiwara, A., Abe, T., Hashimoto, T., Matsuura, H., Takahashi, K., 2012. Efficient synthesis of (+)-*cis*-12-oxo-phytodienoic acid by an *in vitro* enzymatic reaction. Biosci., Biotechnol., Biochem. 76, 2325–2328. https://doi.org/10.1271/bbb.120506.

Kneeshaw, S., Soriano, G., Monte, I., Hamberg, M., Zamarreño, A.M., García-Mina, J.M., Franco-Zorrilla, J.M., Kato, N., Ueda, M., Rey-Stolle, M.F., Barbas, C., Michavila, S., Gimenez-Ibanez, S., Jimenez-Aleman, G.H., Solano, R., 2022. Ligand diversity contributes to the full activation of the jasmonate pathway in *Marchantia polymorpha*. Proc. Natl. Acad. Sci. U.S.A. 119, e2202930119 https://doi.org/10.1073/pnas.2202930119.

Knieper, M., Vogelsang, L., Guntelmann, T., Sproß, J., Gröger, H., Viehhauser, A., Dietz, K.-J., 2022. OPDAylation of thiols of the redox regulatory network in vitro. Antioxidants 11, 855. https://doi.org/10.3390/antiox11050855.

Koo, A.J.K., Gao, X.L., Jones, A.D., Howe, G.A., 2009. A rapid wound signal activates the systemic synthesis of bioactive jasmonates in Arabidopsis. Plant J. 59, 974–986. https://doi.org/10.1111/j.1365-313X.2009.03924.x.

Liu, W.S., Park, S.W., 2021. 12-oxo-phytodienoic acid: a fuse and/or switch of plant growth and defense responses? Front. Plant Sci. 12, 724079 https://doi.org/10.3389/fpls.2021.724079.

Löwe, J., Dietz, K.-J., Gröger, H., 2020. From a biosynthetic pathway toward a biocatalytic process and chemocatalytic modifications: three-step enzymatic cascade to the plant metabolite *cis*-(+)-12-OPDA and metathesis-derived products. Adv. Sci. 7, 1902973 https://doi.org/10.1002/advs.201902973.

Matuszewski, B.K., Constanzer, M.L., Chavez-Eng, C.M., 2003. Strategies for the assessment of matrix effect in quantitative bioanalytical methods based on HPLC-MS/MS. Anal. Chem. 75, 3019–3030. https://doi.org/10.1021/ac020361s.

Maynard, D., Gröger, H., Dierks, T., Dietz, K.-J., 2018. The function of the oxylipin 12-oxophytodienoic acid in cell signaling, stress acclimation, and development. J. Exp. Bot. 69, 5341–5354. https://doi.org/10.1093/jxb/ery316.

Milman, B.L., 2015. General principles of identification by mass spectrometry. Trac. Trends Anal. Chem. 69, 24–33. https://doi.org/10.1016/j.trac.2014.12.009.
Monte, I., Ishida, S., Zamarreño, A.M., Hamberg, M., Franco-Zorrilla, J.M., García-Casado, G., Gouhier-Darimont, C., Reymond, P., Takahashi, K., García-Mina, J.M., Nishihama, R., Kohchi, T., Solano, R., 2018. Ligand-receptor co-evolution shaped the jasmonate pathway in land plants. Nat. Chem. Biol. 14, 480–488. https://doi.org/10.1038/s41589-018-0033-4.
Monte, I., Kneeshaw, S., Franco-Zorrilla, J.M., Chini, A., Zamarreno, A.M., Garcia-Mina, J.M., Solano, R., 2020. An ancient COI1-independent function for reactive electrophilic oxylipins in thermotolerance. Curr. Biol. 30, 962–971. https://doi.org/10.1016/j.cub.2020.01.023.
Novák, O., Henyková, E., Sairanen, I., Kowalczyk, M., Pospíšil, T., Ljung, K., 2012. Tissue-specific profiling of the *Arabidopsis thaliana* auxin metabolome. Plant J. 72, 523–536. https://doi.org/10.1111/j.1365-313X.2012.05085.x.
Novák, O., Napier, R., Ljung, K., 2017. Zooming in on plant hormone analysis: tissue- and cell-specific approaches. In: Merchant, S.S. (Ed.), Annual Review of Plant Biology, vol. 68. Annual Reviews, Palo Alto, CA, USA, pp. 323–348. https://doi.org/10.1146/annurev-arplant-042916-040812.
Ohkama-Ohtsu, N., Sasaki-Sekimoto, Y., Oikawa, A., Jikumaru, Y., Shinoda, S., Inoue, E., Kamide, Y., Yokoyama, T., Hirai, M.Y., Shirasu, K., Kamiya, Y., Oliver, D.J., Saito, K., 2011. 12-Oxo-phytodienoic acid-glutathione conjugate is transported into the vacuole in Arabidopsis. Plant Cell Physiol. 52, 205–209. https://doi.org/10.1093/pcp/pcq181.
Park, S.-W., Li, W., Viehhauser, A., He, B., Kim, S., Nilsson, A.K., Andersson, M.X., Kittle, J.D., Ambavaram, M.M.R., Luan, S., Esker, A.R., Tholl, D., Cimini, D., Ellerström, M., Coaker, G., Mitchell, T.K., Pereira, A., Dietz, K.-J., Lawrence, C.B., 2013. Cyclophilin 20-3 relays a 12-oxo-phytodienoic acid signal during stress responsive regulation of cellular redox homeostasis. Proc. Natl. Acad. Sci. U.S.A. 110, 9559–9564. https://doi.org/10.1073/pnas.1218872110.
Reymond, P., Weber, H., Damond, M., Farmer, E.E., 2000. Differential gene expression in response to mechanical wounding and insect feeding in Arabidopsis. Plant Cell 12, 707–719. https://doi.org/10.1105/tpc.12.5.707.
Rochat, B., 2017. Proposed confidence scale and ID score in the identification of known-unknown compounds using high resolution MS data. J. Am. Soc. Mass Spectrom. 28, 709–723. https://doi.org/10.1007/s13361-016-1556-0.
Sheard, L.B., Tan, X., Mao, H.B., Withers, J., Ben-Nissan, G., Hinds, T.R., Kobayashi, Y., Hsu, F.F., Sharon, M., Browse, J., He, S.Y., Rizo, J., Howe, G.A., Zheng, N., 2010. Jasmonate perception by inositol-phosphate-potentiated COI1-JAZ co-receptor. Nature 468, 400–405. https://doi.org/10.1038/nature09430.
Shinya, T., Miyamoto, K., Uchida, K., Hojo, Y., Yumoto, E., Okada, K., Yamane, H., Galis, I., 2022. Chitooligosaccharide elicitor and oxylipins synergistically elevate phytoalexin production in rice. Plant Mol. Biol. 109, 595–609. https://doi.org/10.1007/s11103-021-01217-w.
Staswick, P.E., Serban, B., Rowe, M., Tiryaki, I., Maldonado, M.T., Maldonado, M.C., Suza, W., 2005. Characterization of an Arabidopsis enzyme family that conjugates amino acids to indole-3-acetic acid. Plant Cell 17, 616–627. https://doi.org/10.1105/tpc.104.026690.
Staswick, P.E., Tiryaki, I., 2004. The oxylipin signal jasmonic acid is activated by an enzyme that conjugates it to isoleucine in Arabidopsis. Plant Cell 16, 2117–2127. https://doi.org/10.1105/tpc.104.023549.
Staswick, P.E., Tiryaki, I., Rowe, M.L., 2002. Jasmonate response locus JAR1 and several related Arabidopsis genes encode enzymes of the firefly luciferase superfamily that show activity on jasmonic, salicylic, and indole-3-acetic acids in an assay for adenylation. Plant Cell 14, 1405–1415. https://doi.org/10.1105/tpc.000885.
Stelmach, B.A., Muller, A., Hennig, P., Gebhardt, S., Schubert-Zsilavecz, M., Weiler, E.W., 2001. A novel class of oxylipins, *sn*1-*O*-(12-oxophytodienoyl)-*sn*2-*O*-(hexadecatrienoyl)-monogalactosyl diglyceride, from *Arabidopsis thaliana*. J. Biol. Chem. 276, 12832–12838. https://doi.org/10.1074/jbc.M010743200.
Stintzi, A., Weber, H., Reymond, P., Browse, J., Farmer, E.E., 2001. Plant defense in the absence of jasmonic acid: the role of cyclopentenones. Proc. Natl. Acad. Sci. U.S.A. 98, 12837–12842. https://doi.org/10.1073/pnas.211311098.
Stumpe, M., Göbel, C., Faltin, B., Beike, A.K., Hause, B., Himmelsbach, K., Bode, J., Kramell, R., Wasternack, C., Frank, W., Reski, R., Feussner, I., 2010. The moss *Physcomitrella patens* contains cyclopentenones but no jasmonates: mutations in allene oxide cyclase lead to reduced fertility and altered sporophyte morphology. New Phytol. 188, 740–749. https://doi.org/10.1111/j.1469-8137.2010.03406.x.
Šimura, J., Antoniadi, I., Široká, J., Tarkowská, D., Strnad, M., Ljung, K., Novák, O., 2018. Plant hormonomics: multiple phytohormone profiling by targeted metabolomics. Plant Physiol. 177, 476–489. https://doi.org/10.1104/pp.18.00293.
Široká, J., Brunoni, F., Pěnčík, A., Mik, V., Žukauskaitė, A., Strnad, M., Novák, O., Floková, K., 2022. High-throughput interspecies profiling of acidic plant hormones using miniaturised sample processing. Plant Methods 18, 122. https://doi.org/10.1186/s13007-022-00954-3.
Tarkowská, D., Novák, O., Floková, K., Tarkowski, P., Turečková, V., Grúz, J., Rolčík, J., Strnad, M., 2014. Quo vadis plant hormone analysis? Planta 240, 55–76. https://doi.org/10.1007/s00425-014-2063-9.
Thines, B., Katsir, L., Melotto, M., Niu, Y., Mandaokar, A., Liu, G.H., Nomura, K., He, S. Y., Howe, G.A., Browse, J., 2007. JAZ repressor proteins are targets of the SCF^{COI1} complex during jasmonate signalling. Nature 448, 661–665. https://doi.org/10.1038/nature05960.
Turečková, V., Novák, O., Strnad, M., 2009. Profiling ABA metabolites in *Nicotiana tabacum* L. leaves by ultra-performance liquid chromatography-electrospray tandem mass spectrometry. Talanta 80, 390–399. https://doi.org/10.1016/j.talanta.2009.06.027.
Wasternack, C., Feussner, I., 2018. The oxylipin pathways: biochemistry and function. In: Merchant, S.S. (Ed.), Annual Review of Plant Biology, vol. 69. Annual Reviews, Palo Alto, CA, USA, pp. 363–386. https://doi.org/10.1146/annurev-arplant-042817-040440.
Wasternack, C., Hause, B., 2013. Jasmonates: biosynthesis, perception, signal transduction and action in plant stress response, growth and development. An update to the 2007 review in. Annals of Botany. Ann. Bot 111, 1021–1058. https://doi.org/10.1093/aob/mct067.
Wasternack, C., Song, S.S., 2017. Jasmonates: biosynthesis, metabolism, and signaling by proteins activating and repressing transcription. J. Exp. Bot. 68, 1303–1321. https://doi.org/10.1093/jxb/erw443.
Weber, H., Vick, B.A., Farmer, E.E., 1997. Dinor-oxo-phytodienoic acid: a new hexadecanoid signal in the jasmonate family. Proc. Natl. Acad. Sci. U.S.A. 94, 10473–10478. https://doi.org/10.1073/pnas.94.19.10473.
Westfall, C.S., Muehler, A.M., Jez, J.M., 2013. Enzyme action in the regulation of plant hormone responses. J. Biol. Chem. 288, 19304–19311. https://doi.org/10.1074/jbc.R113.475160.
Westfall, C.S., Sherp, A.M., Zubieta, C., Alvarez, S., Schraft, E., Marcellin, R., Ramirez, L., Jez, J.M., 2016. *Arabidopsis thaliana* GH3.5 acyl acid amido synthetase mediates metabolic crosstalk in auxin and salicylic acid homeostasis. Proc. Natl. Acad. Sci. U.S.A. 113, 13917–13922. https://doi.org/10.1073/pnas.1612635113.
Yamamoto, Y., Ohshika, J., Takahashi, T., Ishizaki, K., Kohchi, T., Matusuura, H., Takahashi, K., 2015. Functional analysis of allene oxide cyclase, MpAOC, in the liverwort *Marchantia polymorpha*. Phytochemistry 116, 48–56. https://doi.org/10.1016/j.phytochem.2015.03.008.
Zimmerman, D.C., Feng, P., 1978. Characterization of a prostaglandin-like metabolite of linolenic acid produced by a flax-seed extract. Lipids 13, 313–316. https://doi.org/10.1007/bf02533720.